Analytical Investigations of Coupled Rotorcraft/Engine/Drive Train Dynamics

A. Stewart Hopkins and Gene C. Ruzicka
Research Scientists

Robert A. Ormiston
Chief, Rotorcraft Dynamics Division

Aeroflightdynamics Directorate
Aviation Research, Development and Engineering Center
U.S. Army Aviation and Troop Command
Ames Research Center
Moffett Field, California

Abstract

The fundamental characteristics of the coupled rotor, engine, and drive train dynamics of a rotorcraft are investigated with two different analytical models. A detailed finite element model of a complete vehicle including flexible rotor blades, fuselage, engine, transmission, tail rotor, and a feedback control system was studied with the Second Generation Comprehensive Helicopter Analysis System (2GCHAS). To complement and aid in interpreting the comprehensive analysis results, a simpler five degree of freedom analysis, Rotor/Engine/Drive Train (REDT), was developed to perform rapid parametric analyses and illustrate system dynamic behavior. Eigenanalysis results including frequencies, damping, and mode shapes are presented for the linearized system without the effects of rotor aerodynamics. Closed form solutions for limiting cases were found to be helpful in understanding the modes.

Notation

C	damping matrix
C_B	blade lag damping
C_E	engine effective damping
e	distance from rotor center to blade hinge
F	applied moments
G	engine feedback gain
i	$\sqrt{-1}$
I_E	engine torsional moment of inertia
I_F	fuselage torsional moment of inertia
I_H	rotor hub torsional moment of inertia
I_{Rc}	rotorcraft torsional moment of inertia $= I_F + I_{Rtr} + I_T + I_E$
I_{Rtr}	rotor torsional moment of inertia $= N_b M_b(\frac{l^2}{3} + le + e^2) + I_H$
I_T	transmission torsional moment of inertia
I_{TTR}	transmission torsional moment of inertia without tail rotor
I_{TR}	tail rotor moment of inertia
K	stiffness matrix
K_B	blade lag spring stiffness
$K_{B\Omega}$	effective blade lag stiffness including centrifugal effects $= K_B + M_B\Omega^2\frac{l}{2}e$
K_E	engine output shaft stiffness
K_S	rotor shaft stiffness
K_{TR}	tail rotor shaft stiffness
l	distance from blade hinge to blade tip
M	mass matrix
M_B	mass of a blade
N	gear ratio of engine speed:rotor speed

Presented at the American Helicopter Society 2nd International Region Aeromechanics Specialists' Conference, Bridgeport, Connecticut, October 11-13, 1995.

N_B	number of blades
N_{TR}	gear ratio of engine speed:tail rotor speed
t	time
T	coordinate transformation matrix
λ	eigenvalue $= \sigma + i\omega$
ω	imaginary part of eigenvalue
Ω	rotor speed
Ω_0	nominal rotor speed
ψ	rotational displacements
σ	real part of eigenvalue
$\dot{(\ )}$	$\frac{d}{dt}(\ )$
$\ddot{(\ )}$	$\frac{d^2}{dt^2}(\ )$
$(\ )'$	in transformed coordinates
$\bar{(\ )}$	normalized by Ω_0

Introduction

The design of modern rotorcraft involves careful integration of the airframe, rotor, engine, drive train, and control system characteristics. Consequences of inadequate integration may include excessive loads in the rotor or drive train components, inadequate maneuvering performance, or unacceptable vehicle handling qualities. A number of examples of these types of problems have been documented in the literature, Refs. [1]–[4]. Most recently the AH-64A Apache experienced difficulties following the introduction of the upgraded T700-GE-701C engine. Whereas the original engine installation was successful, the higher power engine initially caused unsatisfactory rotor speed droop transients and unacceptable handling qualities, Ref. [5].

Such problems arise from the inherent complexity of modern high performance rotorcraft systems and the inadequate analytical tools that prevent the designer from accurately addressing the true nature of interaction phenomena in new rotorcraft. And limited generic research has been done to explore the fundamental behavior of complex rotorcraft dynamic systems and thus to fully appreciate the nature of the problems that the designer may face.

A number of investigators have addressed these problems and developed a wide variety of vehicle and propulsion system models. A detailed nonlinear model of the T700-GE-700 turboshaft engine with components for the compressor, combustor, gas generator, and power turbine, was developed in Ref. [6] for application to real-time helicopter simulation models. A similar engine representation was employed for the detailed helicopter rotor/propulsion system dynamics analysis presented in Ref. [7]. This analysis was used to investigate effects of engine controller characteristics and nonlinearities on transient responses to pilot control inputs. A simplified rotor/drive train analysis based on a linearized version of the Ref. [6] engine model was presented in Ref. [8] and used to investigate variations in rotor aeroelastic characteristics, drive train properties, and feedback gain on system stability and transient response. In Ref. [9], a very simple model of coupled rotor and engine system with effective spring-mass-damper components was used to investigate modeling requirements for drive train torsional stability analysis. Finally, the efforts reported in Ref. [5] included application of a detailed model of the vehicle, propulsion, and flight control system for investigation of airframe/engine integration issues of the T700-GE-701C Apache upgrade.

Only recently have comprehensive analysis tools for rotorcraft aeromechanics such as the Second Generation Comprehensive Helicopter Analysis System (2GCHAS), Refs. [10]–[13], become available that provide for general treatment of finite element structural models and sophisticated aerodynamic models, together with the capability to include propulsion system/drive train and flight/engine control system representations. While, in many cases, the investigations cited above employ sophisticated models, and address a variety of engine/airframe interaction phenomena, there are many other details of the problem that deserve attention. The purpose of this paper is to study the dynamic interactions of the coupled rotor/vehicle/propulsion/drive train system using the capabilities of 2GCHAS and a simplified analytical model. The investigation will thus address eigensolution frequency, damping, and mode shape results for the linearized structural dynamic and propulsion system models and will not address time domain transient responses arising from pilot control inputs or aerodynamic excitations.

The paper will demonstrate specific 2GCHAS capabilities pertaining to rotorcraft/propulsion system dynamic analysis and present representative results in the course of investigating the complex dynamic interactions for a reasonably high fidelity model of the physical system. The paper will show how this can be facilitated with a simplified five degree of freedom Rotor/Engine/Drive Train (REDT) model to help confirm and interpret the 2GCHAS results. The REDT analysis will be used to explore the effects of several configuration parameters and also to derive approximate closed form solutions for frequency and damping of key system modes for clarifing some of the basic features of the system. The paper will illustrate how the comprehensive, simplified, and closed form analytical approaches complement one another in achieving the overall objectives of this work.

The paper first describes the comprehensive and simplified analytical models. Next, the nominal articulated rotor helicopter configuration, will be defined and nominal results presented for both analyses. Closed form solutions for limiting cases of the REDT model are derived and correlated with the nominal results. Some of the more interesting behaviors of the system are investigated by varying system parameters in both the simplified and comprehensive models. These include the blade lag damper, lag hinge stiffness (to model a hingeless rotor), engine inertia and damping, tail rotor dynamics, and engine feedback gain.

2GCHAS Comprehensive Model

The Second Generation Comprehensive Helicopter Analysis System (2GCHAS) is a comprehensive multidisciplinary, computer software system for predicting rotorcraft aeromechanics characteristics. 2GCHAS was developed by the U.S. Army to integrate the major rotorcraft technical disciplines to provide interdisciplinary analytical capabilities for a broad spectrum of researchers, designers, and evaluators. A broad overview of the system capabilities is available in Ref. [10]. A key feature of 2GCHAS is that the structural model is finite element based, which allows the user to specify the model configuration in the input data, and changing the model can be done without altering the source code.

The 2GCHAS model used in this study is based on test problem Chapter 19 in the 2GCHAS Applications Manual, Ref. [13]. The model combines simple rotor, airframe, engine/drive train and control components into a single rotorcraft model. It is intended to illustrate 2GCHAS' capability to model a multicomponent, single rotor helicopter, and to analyze the dynamic couplings among its constituent components. The model's rotor and airframe are patterned after the UH-60, which is representative of a wide variety of rotorcraft. It has a four-bladed articulated rotor with conventional hydraulic lag dampers. The comprehensive engine model is based on the T700-GE-700 turboshaft engine, which has been used in both the Apache and UH-60 rotorcraft.

The comprehensive model follows the four-level hierarchy required for all 2GCHAS models. The top level is the system itself, and the levels beneath that are subsystem, primitive, and element. A subsystem must be a fuselage, a rotor, or a control subsystem. Primitives are convenient groupings of elements within subsystems. Elements are structural components whose attributes are explicitly coded in the software, embody the fundamental mechanical and structural attributes needed to model all aspects of rotorcraft behavior. Also provided in 2GCHAS is a constraint library, which represent couplings among the the structural components. Constraints may be applied at any level of the model hierarchy. Brief descriptions of the elements and constraints used in the comprehensive model are included with the model descriptions that follows.

The rotor and fuselage portions of the airframe, (Fig. 1), are briefly described here. These are identical to those used in Chapter 19 of Ref. [13], and more detailed descriptions—including listings of the element properties—may be found there. The rotor subsystem contains four articulated blades, with coincident lead-lag and flap hinges at 4.66% offset. Each blade is a primitive of the rotor subsystem, and contains two nonlinear beam elements, one on either side of the hinge. The nonlinear beam element is used in 2GCHAS to model the aeroelastic properties of rotor blades, including the lag-flap-pitch couplings resulting from finite blade rotations.

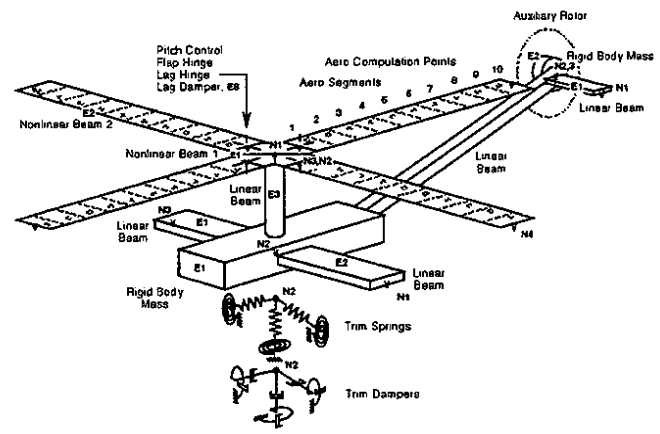

Figure 1: Single Rotor Helicopter Airframe and Rotor Model

The fuselage subsystem consists of an airframe and an engine/drive train. The lifting surfaces of the airframe are a main wing and a horizontal rear stabilizer, each modeled as a primitive. Their structural characteristics are represented with linear beam elements, which are simpler and computationally less expensive than the nonlinear beam. The remainder of the fuselage, which includes the engine/drive train, fuselage body, rotor mast and tail boom, are modeled in a single primitive. The translational and in-plane rotational inertias of the tail rotor are incorporated into the airframe using a rigid body mass element, while the torsional inertia of the tail rotor is included with the engine/drive train. The tail boom is represented by a linear beam element, and the bulk of the nonstructural inertia of the fuselage is lumped in a rigid body mass element at the base of the rotor mast.

The trim springs and trim dampers shown in Fig. 1 are not elements, but are damping and stiffness terms that stabilize the system equations during the analysis of trim and static equilibrium. They are removed during the eigenanalysis of the linearized system equations, and do not affect the frequency and damping results presented in this study.

The engine/drive train (Fig. 2) consists of a torque

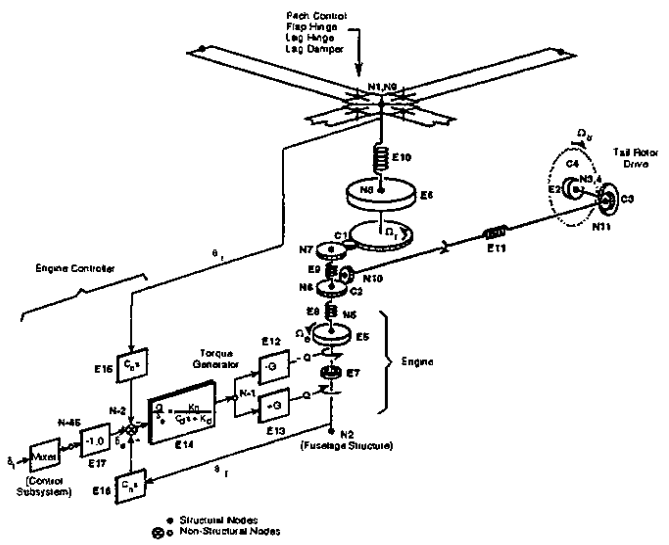

Figure 2: Engine/Drive Train Model

generator and a mechanical engine/drive train model. The torque generator models the generation of engine torque in response to the engine throttle control. It uses 2GCHAS transfer function elements to model the engine torque dynamics (E14), and to transfer the torque to the fuselage (E12) and to the engine (E13). Additional transfer function elements (E15 and E16) feed back the engine and fuselage responses to the engine controller.

The mechanical model uses spring, damper and rigid body mass elements to model the one-dimensional torsional dynamics of the engine/drive train. The model includes an engine mass (E5), engine shaft springs (E8, E9), a rotor shaft spring (E10) and a transmission mass (E6). The tail rotor consists of a spring (E10) and a torsional inertia (E2). The engine damper (E7) represents damping within the engine/drive train and aerodynamic damping, i.e., resistance offered by gases flowing through the engine to changes in turbine spin rate.

The engine/drive train includes four 2GCHAS multipoint constraints, (C1–C4). Constraint (C1) represents the gear reduction from the engine speed to the rotor shaft speed. As explained in Ref. [11], this constraint, and all gear reduction constraints, apply to elastic rotations of the components relative to the fuselage structure. Thus, the constraint (C1) reduces the relative vertical rotations of nodes (N7) and (N2) by a factor of N to obtain the relative vertical rotations of nodes (N8) and (N2). Constraint (C2) reduces engine speed to tail rotor speed, and changes the drive train spin direction from vertical to longitudinal. Mathematically, this involves reducing the relative vertical rotations of nodes (N6) and (N2), by a factor of N_{TR} to obtain the relative horizontal rotations of nodes (N10) and (N2). Constraint (C3) reorients the drive train spin direction from longitudinal to sideways, and couples the torsional motion of the tail rotor (located at node (N4)) to the drive train node (N3). Mathematically, this equates the relative side rotations of nodes (N4) and (N3) to the relative longitudinal rotations of nodes (N11) and (N3). Constraint (C4) simply attaches the tail rotor degrees of freedom (other than the torsional rotation) to node (N3) on the airframe. The model contains 39 elements and 115 degrees of freedom.

REDT Simplified Model

The simplified Rotor Engine Drive Train (REDT) model, Fig. 3, was developed to facilitate understanding of the

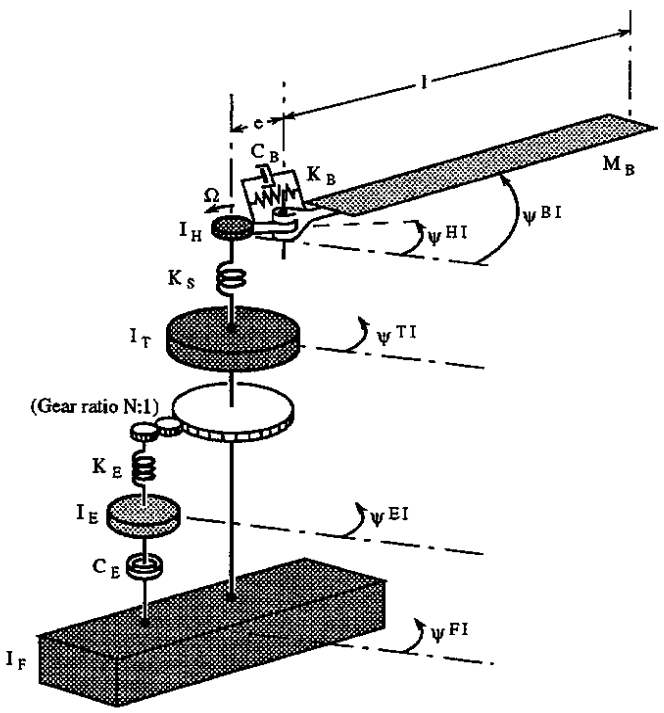

Figure 3: REDT model (one of N_B blades).

dynamic behavior of the 2GCHAS comprehensive model by abstracting its salient characteristics. This model was simple enough that it permitted closed form solutions in limiting cases. It also served as the basis for a highly interactive, computer program (also called REDT) that permitted the extensive exploration of the space of model parameters necessary for gaining a full understanding of the complex dynamics of the system. The program supported highly interactive parameter modification, very short run times and immediate on screen plotting of results.

The REDT model consists of five rotational degrees of freedom: the collective lead-lag rotation of the blades, the hub, the transmission output, the rotating part of the engine, and the fuselage. The blades are connected to the hub through an offset hinge, spring, and damper. The hub is connected to the transmission output through a shaft spring. The transmission output is free to rotate in the fuselage but connected to the engine through a reduction gear and a spring. The engine is free to rotate in the fuselage through a damper.

Many of the REDT model parameters are identical to the properties of the 2GCHAS elements: C_B and E6, K_S and E10, N and C1, I_E and E5, and C_E and E7. The REDT lengths l and e are the same as the distance between the appropriate nodes in the 2GCHAS model. The REDT blade is a rigid approximation to the flexible 2GCHAS blade with the same mass, M_B. Similarly, I_H and I_F are rigid approximations with the same inertia as the appropriate collection of 2GCHAS flexible and rigid elements. The tail rotor shaft, E11 with stiffness K_{TR}, was treated as rigid in the REDT model, allowing the flexibilities of the two engine springs E8 and E9 in 2GCHAS to be combined into K_E in REDT. The 2GCHAS tail rotor inertia, I_{TR} from element E2, was lumped with the transmission inertia without the tail rotor, I_{TTR} from element E6, accounting for the engine:tail rotor gear ratio, N_{TR} from constraint C2, into the REDT transmission inertia $I_T = I_{TTR} + (\frac{N}{N_{TR}})^2 I_{TR}$. The REDT model includes a blade lag-spring, K_B, not present in the 2GCHAS model.

A virtual work approach was used to develop the kinematically non-linear equations of motion for the model. The equations were linearized about a state consisting of no deformation but a steady rotational velocity of the rotor, drive train, and engine (at a geared up rotational velocity).

The rotational displacement ψ vector is:

$$\begin{Bmatrix} \psi^F \\ \psi^E \\ \psi^T \\ \psi^H \\ \psi^B \end{Bmatrix} = \begin{Bmatrix} \psi^{FI} \\ \psi^{EI}/N - \Omega t \\ \psi^{TI} - \Omega t \\ \psi^{HI} - \Omega t \\ \psi^{BI} - \Omega t \end{Bmatrix} \tag{1}$$

that is the fuselage, transmission, hub and blade rotational displacements are the rotation relative to inertial space less the rotational speed of that component multiplied by time. The engine rotational displacement is treated differently. Because of the gear ratio, a unit displacement of the transmission is in some sense equivalent to N units of engine displacement. Especially for visualizing mode shapes, it is convenient to select the engine coordinate so that $\psi^{EI} = N\Omega t + N\psi^E$.

The result of linearization is a set of second order ordinary differential equations of the form:

$$M\ddot{\psi} + C\dot{\psi} + K\psi = F \tag{2}$$

where the mass (M) matrix is:

$$\begin{bmatrix} I_F & 0 & 0 & 0 & 0 \\ 0 & N^2 I_E & 0 & 0 & 0 \\ 0 & 0 & I_T & 0 & 0 \\ 0 & 0 & 0 & N_B M_B e^2 + I_H & N_B M_B \frac{l}{2} e \\ 0 & 0 & 0 & N_B M_B \frac{l}{2} e & N_B M_B \frac{l^2}{3} \end{bmatrix} \tag{3}$$

the damping (C) matrix is:

$$\begin{bmatrix} C_E & -NC_E & 0 & 0 & 0 \\ -NC_E & N^2 C_E & 0 & 0 & 0 \\ 0 & 0 & 0 & 0 & 0 \\ 0 & 0 & 0 & N_B C_B & -N_B C_B \\ 0 & 0 & 0 & -N_B C_B & N_B C_B \end{bmatrix} \tag{4}$$

and the stiffness (K) matrix is:

$$\begin{bmatrix} (N-1)^2 K_E & N(N-1)K_E & -N(N-1)K_E & 0 & 0 \\ N(N-1)K_E & N^2 K_E & -N^2 K_E & -K_S & 0 \\ -N(N-1)K_E & -N^2 K_E & N^2 K_E + K_S & 0 & 0 \\ 0 & 0 & -K_S & K_S + N_B K_{B\Omega} & -N_B K_{B\Omega} \\ 0 & 0 & 0 & -N_B K_{B\Omega} & N_B K_{B\Omega} \end{bmatrix} \tag{5}$$

Results for Nominal Configuration

The nominal configuration for the 2GCHAS comprehensive model and the REDT simplified model are defined by the parameters presented in Table 1.

2GCHAS Nominal Results

The 2GCHAS analysis of the nominal model gives the eigenvalues for the full system. Figure 4 shows the frequency and damping plots from the 2GCHAS analysis. Immediately apparent in the frequency plot are sets of fundamental flap modes, with "F1C," "F1D," and "F1P"

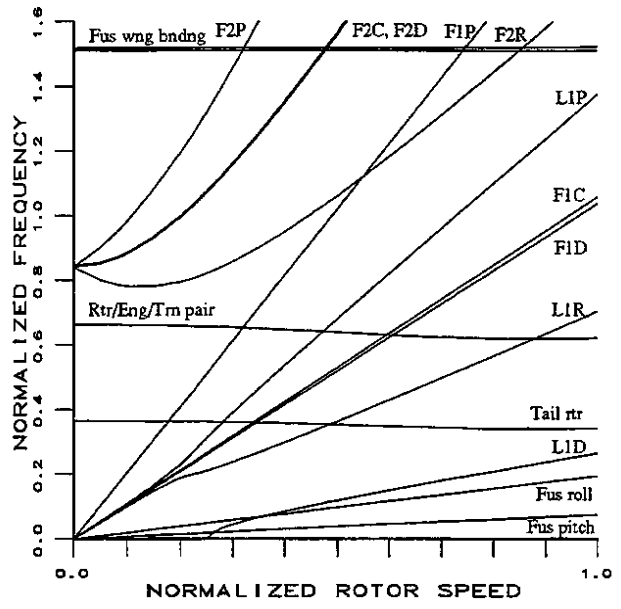

(a) Frequency

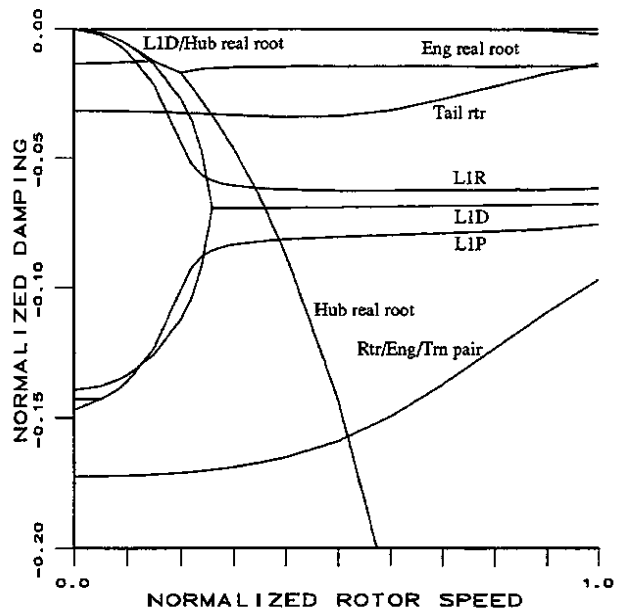

(b) Damping

Figure 4: Eigenvalues for Nominal 2GCHAS Model

Parameter	2GCHAS	Value	Units
C_B	E6	5933.3	ft-lb-sec/rad
C_E	E7	0.34	ft-lb-sec/rad
e		1.25	ft
G	E12, E13	10	
I_E	E5	.124	slug-ft^2
I_F		41900.3	slug-ft^2
I_H		40	slug-ft^2
I_{Rc}		50082.3	slug-ft^2
I_{Rtr}		7531.91	slug-ft^2
I_T		650	slug-ft^2
I_{TTR}	E6	218.14	slug-ft^2
I_{TR}	E2	19.69	slug-ft^2
K_B		0	ft-lb/rad
K_E		6000	ft-lb/rad
$2K_E$	E8	12000	ft-lb/rad
$2K_E$	E9	12000	ft-lb/rad
K_S	E10	273106	ft-lb/rad
K_{TR}	E11	2000	ft-lb/rad
l		25.58	ft
M_B	E2	7.4428	slug
N	C1	80	
N_B		4	
N_{TR}	C2	17.5792	
Ω_0		27	rad/sec

Table 1: Parameter values for nominal configuration.

denoting the collective, differential collective, and progressing modes. Also seen are the first elastic flap modes, with "F2R," "F2C," "F2D," and "F2P," denoting the regressing, collective, differential collective and progessing modes. The fundamental flap regressing mode couples with the pitch and roll motion of the fuselage in the "Fus pitch" and "Fus roll" modes. The increase in frequency of these modes with with rotor speed reflects rotor gyroscopic effects. The "Fus wng bndng" mode represents bending oscillation of the wing, and is essentially uncoupled from the rotor. The familiar differential collective, regressing and progressing lag modes are labeled "L1D," "L1R," and "L1P," respectively. These modes exert no torque about the hub, and are therefore unaffected by the engine/drive train. An effect of the lag damper is the transition of the "L1D" mode from a conjugate pair to two real roots at $\overline{\Omega} = .25$. This phenomenon is most apparent in the damping plot, where "L1D" branches into two roots at the transition point. An isolated collective lag frequency does not appear because that mode couples with the engine/drive train. The "Rtr/Eng/Trn pair" embodies the most significant rotor/engine/drive train/fuselage coupling. It mostly represents coupling between the engine/drive train and the fundamental collective lag mode, and a more explicit label could be

"L1C/Eng/Trn pair."

There are several engine/drive train structural dynamic modes, but some are outside the frequency range of Fig. 4. The "Tail rtr" mode is predominantly torsional oscillation of the tail rotor. One "Hub real root" representing mostly hub motion is visible, but a companion is off scale.

It is worthwhile to discuss the rigid body modes of the comprehensive model, and their effects on the frequency and damping plots. An unconstrained rotorcraft model—one without an engine/drive train—has six rigid body modes: three translations and three rotations. The three translational modes and rigid body yaw mode have zero frequencies. The "Fus roll" and "Fus pitch" modes, which have already been mentioned, couple fuselage pitch and roll motion with the rotor flap regressing mode. Two remaining rigid body zero roots involve angular displacements without velocity. Since the comprehensive model has an engine/drive train, it has an additional zero frequency mode that involves rotation—without velocity—of the engine/drive train. The "Eng real root," which is seen in the damping plot, may be regarded as a rigid body mode, and would have zero frequency were it not for the engine damper. This mode, which is discussed in more detail in the next section, involves inertia forces of the engine/drive train reacting against the engine damper.

REDT Nominal Results

The characteristics of the roots will now be discussed in more detail using the nominal results for the REDT simplified model. Figure 5 presents the locus of roots with $\overline{\Omega}$. References to roots are based on their character and values at $\overline{\Omega} = 1$. The ten roots of the five degree of freedom system are identified in that figure. Figure 6 and Fig. 7 presents the roots' frequency and damping versus rotor speed. Note the two "Hub real roots" coalesce and become the the complex conjugate "Hub pair" at a point ($\overline{\Omega} \approx 3$) outside the range of $\overline{\Omega}$ in the root-locus plot. Figure 8 presents the mode shapes associated with the roots at $\overline{\Omega} = 1$. The eigenvectors are presented as signed amplitudes and phases in the range $(-\pi/2, \pi/2)$. For real roots, the phases are zero and are not presented. For complex conjugate pairs, only one of the vector of phases is presented and the other is its negative. Note that the degree of freedom ψ^E, Eq. (1), is presented, so the engine displacement is divided by N. Referring to Figs. 5–8, the behavior of the roots for the nominal REDT model will now be interpreted and described.

The "3 rigid body zero roots" on the root-locus plots correspond to a pair of zero roots associated with the "Rotorcraft rigid body yaw" mode and one zero root as-

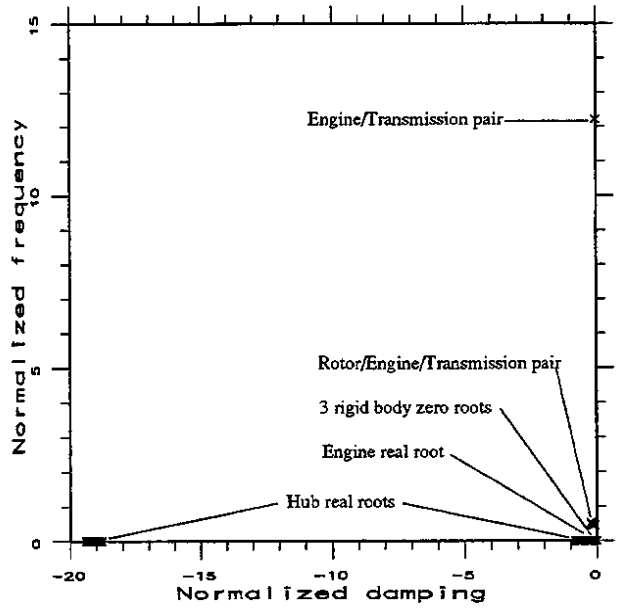

(a) All 10 roots

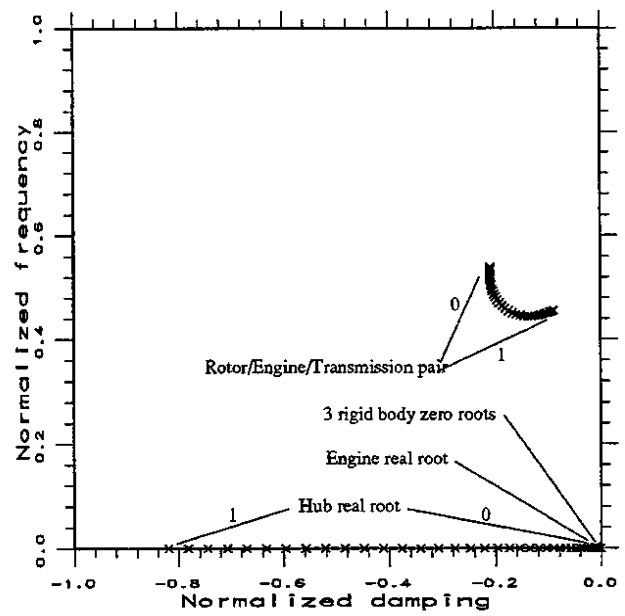

(b) Smaller roots

Figure 5: Root-locus for nominal REDT model.

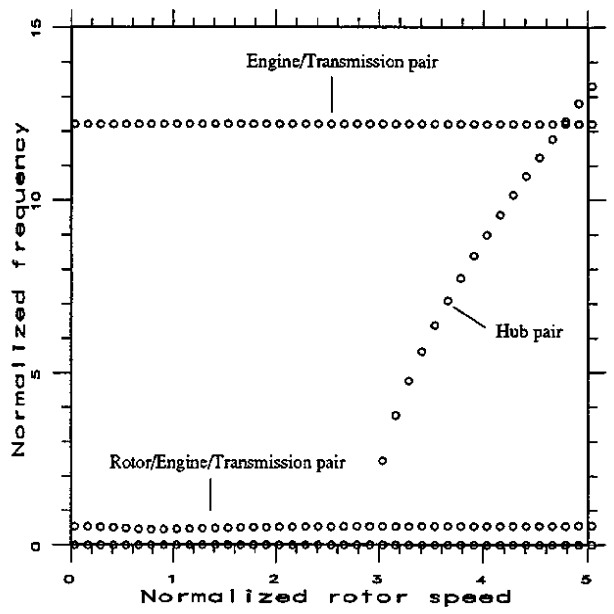

(a) Frequency of all roots

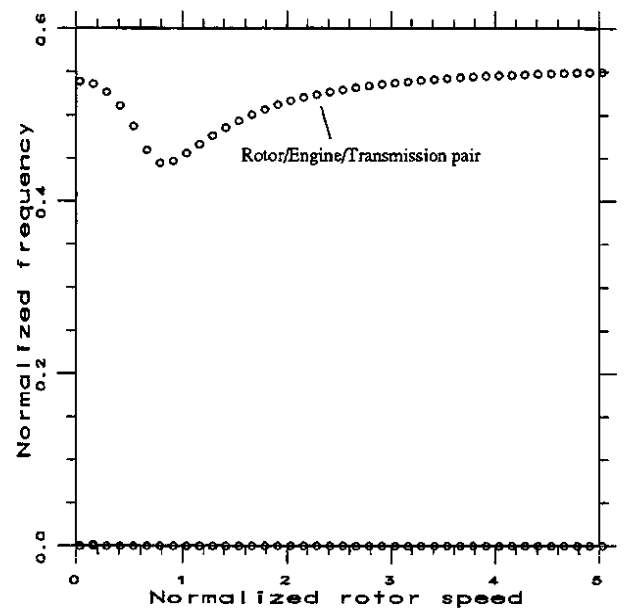

(b) Frequency of smaller roots

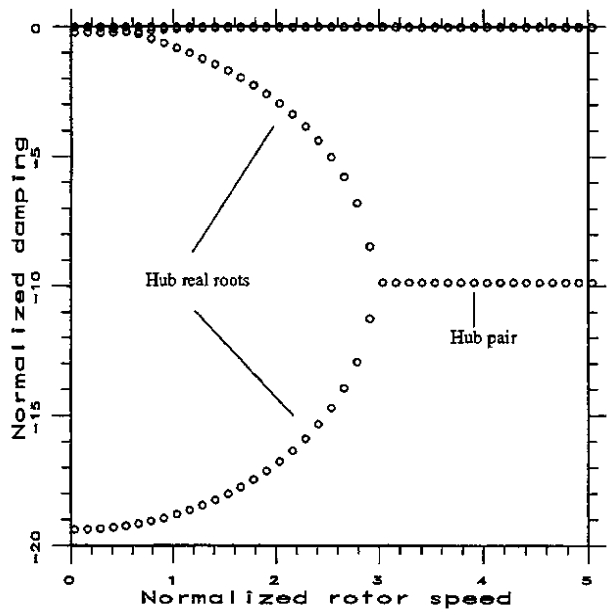

(c) Damping of all roots

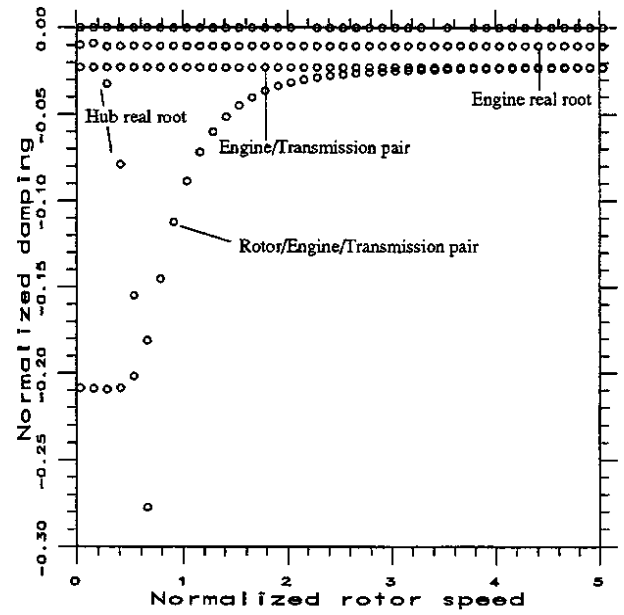

(d) Damping of smaller roots

Figure 6: Eigenvalues for nominal REDT model.

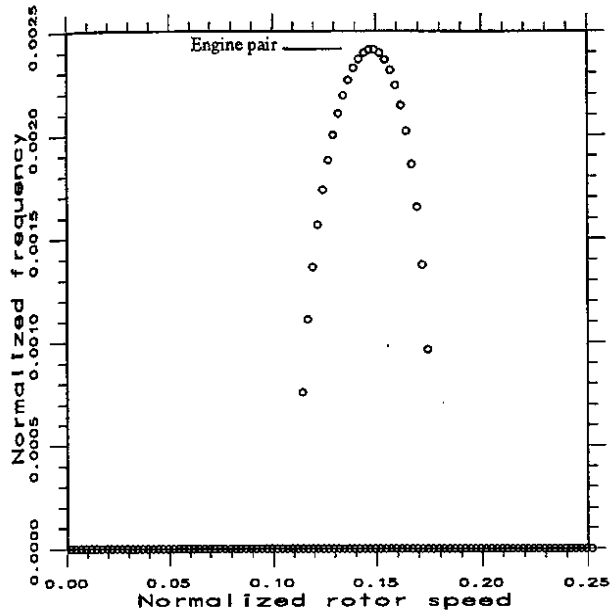

(a) Frequency of smallest roots

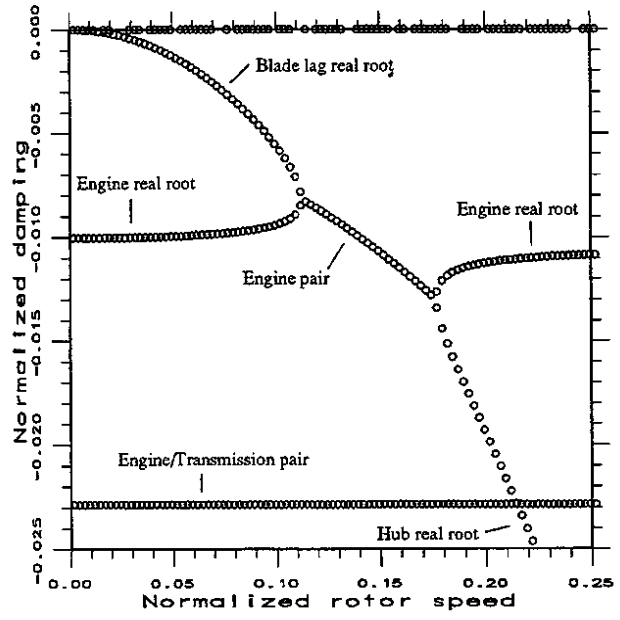

(b) Damping of smallest roots

Figure 7: Eigenvalues for nominal REDT model—Hub and Engine real root coupling.

sociated with the "Rotating system rigid body" mode. These modes neither vary with rotor speed nor couple with other modes. The "Rotorcraft rigid body yaw" mode is the rigid body torsional (yaw) mode of the complete vehicle system (which is unrestrained by external moments). The mode shape has unit amplitude for all displacements, except that (in accord with Eq. (1)) the unit engine motion has been divided by the transmission gear ratio N.

The "Rotating system rigid body" root at zero is closely related to the "Engine real root" at -0.0106. The "Rotating system rigid body" mode shape represents a unit rotation of the rotor and transmission with no fuselage rotation and a corresponding N units of engine rotation, which after dividing by N is plotted as a unit rotation. Were it not for the torque of the engine damper (C_E) located between the rotor/drive train components and the fuselage, there would be a pair of these zero root "Rotating system rigid body" modes. However, with the damper, although a displacement creates no torque (and hence there is one zero root), a unit velocity does create a torque which is reacted by the fuselage and rotating system inertias resulting in the "Engine real root" convergence mode. The "Engine real root" is so named because it is the engine's damping that results in a real root. But, perhaps confusingly, the mode shape involves a rigid rotation of the engine/transmission/rotor, the same as a "Rotating system rigid body" mode with a little opposing rigid body fuselage motion. The damping of the "Engine real root" is essentially constant with rotor speed except when it couples with one of the "Hub real roots" as discussed below. (The "Rotating system rigid body" is the only eigenvector that was manually generated since the computed eigenvectors are less easily understood linear combinations of the three $\lambda = 0$ roots.)

The "Rotor/Engine/Transmission pair" is a complex conjugate pair at $-0.0886 \pm 0.456i$. This is the principal rotor/engine/drive train mode of the system. The mode shape shows significant participation by all of the rotating components. It primarily represents the rotor blade collective lag inertia, I_{Rtr}, reacting against the engine and transmission inertias, I_E and I_T, through the flexibility of the rotor shaft spring, K_S, and the impedance at the blade lag hinge, C_B and $K_{B\Omega}$. Owing to the large inertia of the fuselage, I_F, only small yaw motion is present in this mode. The roots show a continuous variation with rotor speed controlled by dependence of blade lag frequency on rotor speed and the damping contributions of the blade and engine dampers. The roots approach asymptotic values at high rotor speeds. As the impedance at the blade lag hinge increases, the participation of hub in the mode shape (not shown) approaches

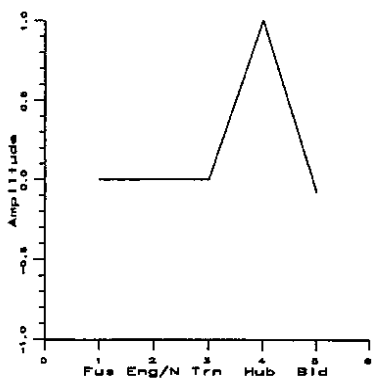

(a) Hub real root
$\overline{\lambda} = -18.8$

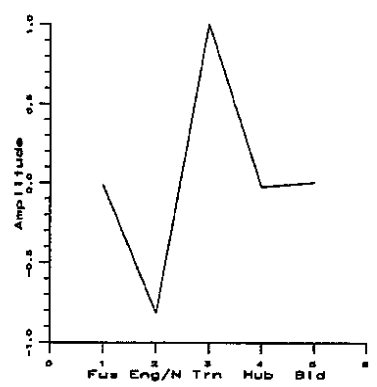

(b) Eng/Trn pair amplitudes
$\overline{\lambda} = -0.0229 \pm 12.08i$

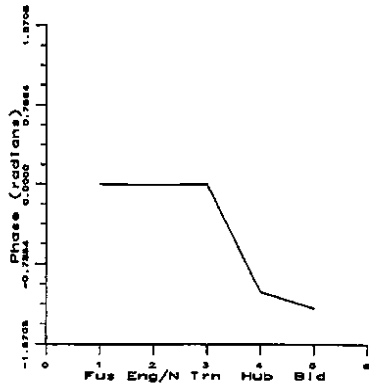

(c) Eng/Trn pair phases
$\overline{\lambda} = -0.0229 \pm 12.08i$

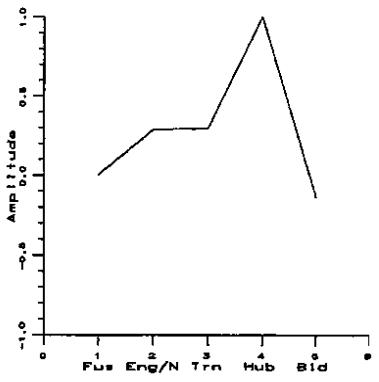

(d) Hub real root
$\overline{\lambda} = -0.820$

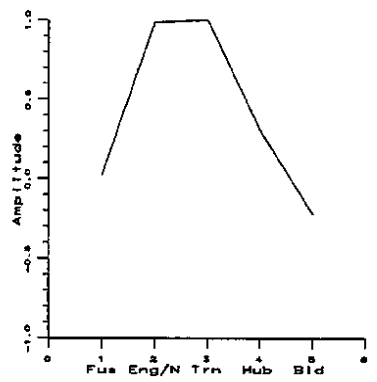

(e) Rtr/Eng/Trn pair amplitudes
$\overline{\lambda} = -0.0886 \pm 0.456i$

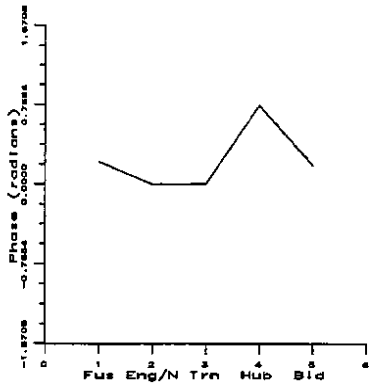

(f) Rtr/Eng/Trn pair phases
$\overline{\lambda} = -0.0886 \pm 0.456i$

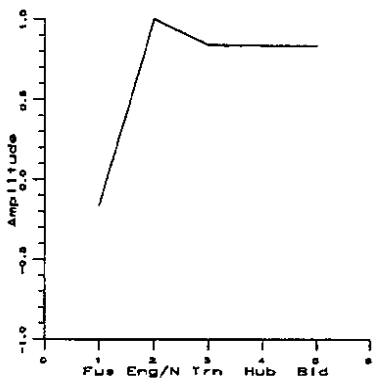

(g) Engine real root
$\overline{\lambda} = -.0106$

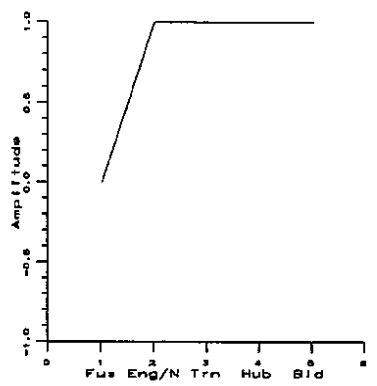

(h) Rotating system rigid body
$\overline{\lambda} = 0$

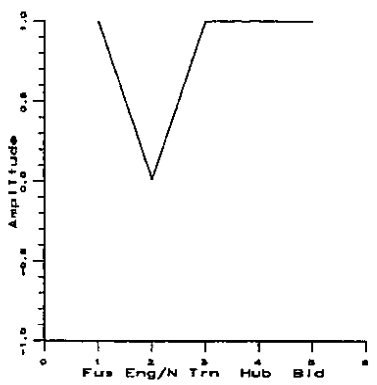

(i) Rotorcraft rigid body yaw pair
$\overline{\lambda} = 0, 0$

Figure 8: Eigenvectors for nominal REDT model at $\overline{\Omega} = 1$

that of the blade. At low rotor speeds, the impedance is controlled by the blade lag damper, C_B, and the participation of the hub in the mode shape (not shown) approaches that of the transmission but with a phase approaching $\pi/2$. This mode does not couple with other modes. Further details of "Rotor/Engine/Transmission pair" mode will be examined in subsequent sections.

The "Engine/Transmission pair" is a complex conjugate pair at $-0.0229 \pm 12.2i$. This is a relatively high frequency and low damping coupled engine/transmission mode. The mode shape is primarily the engine and transmission inertias, I_E and I_T, reacting against each other through the flexibility of the engine output shaft spring, K_E. This is essentially a drive train structural dynamic mode. This root pair is not sensitive to rotor speed and does not couple with other roots in the REDT model.

The "Hub real roots" are a low and high damping real pair at -0.820 and -18.8. Their mode shapes are primarily hub motion reacting in opposition to blade motion. The high damping arises from the strong influence of the blade lag damper, C_B. This mode evolves into the complex conjugate "Hub pair" at $\overline{\Omega} \approx 3.0$. After this point, the frequency increases with rotor speed suggesting that the mode is driven by centrifugal stiffening.

The smaller "Hub real root" couples strongly with the "Engine real root" at $\overline{\Omega} \approx 0.15$. This can be most easily seen in Fig. 7. As $\overline{\Omega}$ decreases the smaller "Hub real root" decreases and approaches zero and the engine participation in its mode shape (not shown) increases. Near $\overline{\Omega} = 0.175$ it interacts strongly with the "Engine real root" and the roots coalesce into an "Engine pair" whose mode shape (not shown) is nearly identical to that of the "Engine real root". Near $\overline{\Omega} = 0.115$ the interaction decreases and the pair again splits into two real roots, the larger of which retains the character of the "Engine real root". The smaller root's mode shape (not shown) becomes almost purely blade lag and is labeled "Blade lag real root" in Fig. 7.

Closed Form Solutions

The use of the simplified REDT model to obtain results for the nominal parameter values increases understanding of the fundamental dynamic behavior of rotorcraft. This analytical model is also used to provide additional insight by developing closed form solutions for the frequency and damping of specific modes—in limiting cases, when approximations can be made, or for certain ranges of parameter values. These closed form expressions may then be used to identify the underlying characteristics of modes appearing in the nominal and parametric results.

Rigid Body and Engine Real Modes

The "Rotorcraft rigid body yaw" zero roots, the "Rotating system rigid body" zero root and the "Engine real root" are uncoupled from the other roots except for the brief coupling with the "Hub real root" at $\overline{\Omega} \approx 0.15$. The uncoupled modes can be approximated by restricting the motion to "rigid body" (non-deformational) motions (i.e., restricting the motion to the subspace defined by the "Rotorcraft rigid body yaw" mode and the "Rotating system rigid body" mode). Let $\psi = T\psi'$ where

$$T = \frac{1}{\sqrt{I_{Rc}}} \begin{bmatrix} 1 & 1 - \frac{I_{Rc}}{I_F - (N-1)I_B} \\ \frac{1}{N} & \frac{1}{N} + \frac{(N-1)I_{Rc}}{N[I_F - (N-1)I_B]} \\ 1 & 1 \\ 1 & 1 \\ 1 & 1 \end{bmatrix} \tag{6}$$

Transforming the mass, damping and stiffness matrices (Eqs. (3), (4) and (5)) by postmultiplying by T and premultiplying by its transpose and then taking the determinant in the generalized eigenvalue problem gives the following equation for the roots

$$\lambda^4\{\gamma^2[I_F + (N-1)^2 I_E] - 1\} + \lambda^3\gamma^2 N^2 C_E = 0 \tag{7}$$

Clearly there is a root at $\lambda = 0$ with a multiplicity of three. The fourth, "Engine real root", is

$$\lambda_4 = \frac{I_{Rc} N^2 C_E}{I_{Rc}[I_F + (N-1)^2 I_E] - [I_F - (N-1)I_E]^2} \tag{8}$$

For most rotorcraft $NI_E << I_{Rc} - I_F$ and the root is approximately

$$\lambda_4 = \frac{I_{Rc} N^2 C_E}{(I_{Rc} - I_F)I_F + (N-1)^2 I_{Rc} I_E} \tag{9}$$

Two zero roots with the first column of Eq. (6) and the third zero root with the second column of Eq. (6) are the exact solution for the "Rotorcraft rigid body yaw" and the "Rotating system rigid body" modes of the full simplified model. Evaluating Eq. (8) at the nominal parameter values gives $\overline{\lambda} = -.01055$ which is very close to the computed value $\overline{\lambda} = -.01058$ at $\overline{\Omega} = 1$. This is a very close approximation to the "Engine real root" (Figs. 6 and 8g).

Engine/Transmission Modes

The "Engine/Transmission pair" is an uncoupled conjugate pair of roots. Guided by the mode shape, the engine, transmission and fuselage are isolated by assuming zero rotor and hub motion and negligible shaft stiffness

($K_S \ll N^2 K_E$). The relevant degrees of freedom are just extracted with the transformation $\psi = T\psi'$ where

$$T = \begin{bmatrix} 1 & 0 & 0 \\ 0 & 1 & 0 \\ 0 & 0 & 1 \\ 0 & 0 & 0 \\ 0 & 0 & 0 \end{bmatrix} \tag{10}$$

Transforming the mass, damping and stiffness matrices (Eqs. (3), (4) and (5)) by postmultiplying by T and premultiplying by its transpose and then taking the determinant in the generalized eigenvalue problem gives the following equation for the roots

$$\begin{aligned} \lambda^3 . \quad \{ \quad & \lambda^3 I_F I_T I_E \\ & +\lambda^2 C_E I_T (I_F + I_E) \\ & +\lambda K_E [I_F I_E N^2 + I_F I_T + I_T I_E (N-1)^2] \\ & +C_E K_E N^2 (I_F + I_T + I_E)\} = 0 \end{aligned} \tag{11}$$

Clearly there is a root at $\lambda = 0$ with a multiplicity of three. The other three roots are found using the cubic formula which is briefly summarized as follows. The characteristic equation can be written as

$$\lambda^3 + p\lambda^2 + q\lambda + r = 0 \tag{12}$$

Letting

$$\lambda = \gamma - p/3 \tag{13}$$

$$a = \frac{1}{3}(3q - p^2) \tag{14}$$

$$b = \frac{1}{27}(2p^3 - 9pq + 27r) \tag{15}$$

reduces the characteristic equation to the form $\gamma^3 + a\gamma + b = 0$. Let

$$A = \sqrt[3]{-\frac{b}{2} + \sqrt{\frac{b^2}{4} + \frac{a^3}{27}}} \tag{16}$$

$$B = \sqrt[3]{-\frac{b}{2} - \sqrt{\frac{b^2}{4} + \frac{a^3}{27}}} \tag{17}$$

then the roots (shifted to γ's) are

$$\gamma_1 = A + B \tag{18}$$

$$\gamma_2 = -\frac{A+B}{2} + \frac{A-B}{2}\sqrt{-3} \tag{19}$$

$$\gamma_3 = -\frac{A+B}{2} - \frac{A-B}{2}\sqrt{-3} \tag{20}$$

and the λ's are recovered by subtracting $p/3$.

Reasonable algebraic expressions can be obtained by making some approximations which are appropriate for typical rotorcraft: $I_T \ll I_F$; $I_E \ll I_F$; and $I_E N^2 \ll I_F$. In addition the engine inertia I_E thought of as a one degree of freedom system with stiffness K_E and damping C_E is typically lightly damped. This means $C_E^2 \ll K_E I_E$ (for the nominal values $0.1 \ll 750.$). From the approximation on C_E, it follows that $\frac{b^2}{4} \ll \frac{a^3}{27}$ which allows A and B to be approximated as

$$A \approx \sqrt{\frac{a}{3}} - \frac{b}{2a} \tag{21}$$

$$B \approx -\sqrt{\frac{a}{3}} - \frac{b}{2a} \tag{22}$$

An algebraic expression for the fourth root is not presented since a much better approximation was obtained previously as Eq. (8). With the above approximations, the following algebraic expressions are obtained for the fifth and sixth "Engine/Transmission pair" roots

$$\lambda_5, \lambda_6 \approx -\frac{C_E I_T}{2I_E(I_E N^2 + I_T)} \pm i\sqrt{\frac{K_E(I_E N^2 + I_T)}{I_E I_T}} \tag{23}$$

Evaluating Eq. (23) gives $\overline{\lambda} = -.0229 \pm 12.14i$ which is very close to the computed values $\overline{\lambda} = -.0229 \pm 12.20i$ at $\overline{\Omega} = 1$. This is a very close approximation to the "Engine/Transmission pair" (Figs. 6 and 8b,c). Inspection of Eq. (23) indicates that the "Engine/Transmission" mode is essentially a free-free mode comprised of the transmission inertia reacting against the engine inertia through the engine shaft spring.

Hub Modes

The "Hub pair" and the larger of the "Hub real roots" are uncoupled from the other roots. The smaller of the "Hub real roots" is briefly and strongly coupled with the "Engine real root" at $\overline{\Omega} \approx 0.15$ and more weakly coupled with the "Rotor/Engine/Transmission pair" for $0 \leq \overline{\Omega} <\sim 1$. Nonetheless, most of the behavior is well approximated by assuming that the rotor is isolated from the rest of the system. Assuming there is zero fuselage, engine and transmission motion, the rotor can be isolated with the transformation $\psi = T\psi'$ where

$$T = \begin{bmatrix} 0 & 0 \\ 0 & 0 \\ 0 & 0 \\ 1 & -N_B M_B(\frac{l^2}{3} + \frac{l}{2}e) \\ 1 & N_B M_B(\frac{l}{2}e + e^2) + I_H \end{bmatrix} \tag{24}$$

Transforming the mass, damping and stiffness matrices (Eqs. (3), (4) and (5)) by postmultiplying by T and premultiplying by its transpose and then taking the determinant in the generalized eigenvalue problem gives the following equation for the roots

$$\begin{aligned} & \lambda^4 \quad M_B \frac{l^2}{3}(I_H + N_B M_B \frac{e^2}{4}) \\ + \quad & \lambda^3 \quad C_B I_{Rtr} \\ + \quad & \lambda^2 \quad K_S M_B \frac{l^2}{3} + K_{B\Omega} I_{Rtr} \\ + \quad & \lambda \quad K_S C_B \\ + \quad & \quad K_S K_{B\Omega} \\ = \quad & 0 \end{aligned} \tag{25}$$

For larger $\overline{\lambda}$ or $\overline{\Omega}$ the rotor can be isolated by assuming K_S is negligible and the rotor is free. In this case, the last two terms vanish and the coefficient of λ^2 becomes $K_{B\Omega} I_{Rtr}$. A factor of λ^2 can be factored out so clearly there is a root at $\lambda = 0$ with a multiplicity of two. Using the quadratic formula, the third and fourth "Hub" roots are

$$\lambda = \frac{-C_B I_{Rtr}}{2M_B \frac{l^2}{3}(I_H + N_B M_B \frac{e^2}{4})} \pm i \cdot \frac{\sqrt{C_B^2 I_{Rtr}^2 - 4M_B \frac{l^2}{3}(I_H + N_B M_B \frac{e^2}{4})(M_B \Omega^2 \frac{l}{2} e + K_B) I_{Rtr}}}{2M_B \frac{l^2}{3}(I_H + N_B M_B \frac{e^2}{4})} \tag{26}$$

Setting the discriminant to zero leads to the critical value for Ω

$$\Omega_{crit} = \sqrt{\frac{2}{M_B l e}} \sqrt{\frac{C_B^2 I_{Rtr}}{4M_B \frac{l^2}{3}(I_H + N_B M_B \frac{e^2}{4})} - K_B} \tag{27}$$

For $\overline{\Omega} > \overline{\Omega}_{crit}$, the real part of the root is

$$\sigma = \frac{-C_B I_{Rtr}}{2M_B \frac{l^2}{3}(I_H + N_B M_B \frac{e^2}{4})} \tag{28}$$

Similarly, for $\overline{\Omega} \to 0$ and $K_B \to 0$, the two roots are real. One is $\lambda_3 = 0$, as is computed. And the other is

$$\lambda_4 = \frac{-C_B I_{Rtr}}{M_B \frac{l^2}{3}(I_H + N_B M_B \frac{e^2}{4})} \tag{29}$$

Finally, the asymptote as $\Omega \to \infty$ of the frequency of the conjugate pair is

$$\omega = \pm i\Omega \sqrt{\frac{3e}{2l}} \sqrt{\frac{I_{Rtr}}{I_H + N_B M_B \frac{e^2}{4}}} \tag{30}$$

which can be thought of as the isolated lag frequency (cf. "Isolated Blade Lag Mode") adjusted for the relaxation of the isolated condition through the hub inertias.

Referring to Fig. 6, the following may be verified. Evaluating Eqs. (27) gives $\overline{\Omega}_{crit} = 3.0$ which is very close to the point at which the computed "Hub real roots" become the "Hub pair". Evaluating Eq. (28) gives $\overline{\sigma} = -9.76$ which is very close to the computed value $\overline{\sigma} = -9.87$ for $\overline{\Omega} > 3$. This is a very close approximation to the "Hub pair" damping. Evaluating Eq. (29) gives $\overline{\lambda} = -19.52$ which is very close to the computed value $\overline{\lambda} = -19.38$ at $\overline{\Omega} = 0$ and can be identified as the y-axis intercept of the lower of the "Hub real roots". Evaluating Eq. (30) gives $\overline{\omega} = 3.25\overline{\Omega}$ which is the asymptote for the "Hub pair". The second column in Eq. (24) provides a good approximation to the mode shape for larger $\overline{\lambda}$. For a unit hub motion the opposing blade motion is approximately $-\frac{3e}{2l}$ or -0.073 which is very close to the computed -0.081 (see Fig. 8a). It is not as good for the smaller of the "Hub real roots" (Fig. 8d).

Isolated Blade Lag Mode

The uncoupled collective lag mode of an N_B-bladed rotor (arising from the isolated lag mode of a single articulated rotor blade) is the principal rotor mode that couples with the engine and drive train components of the rotorcraft. Although the identity of the uncoupled lag mode is largely obscured by participation in the resulting rotor/engine/drive train mode, it is possible to identify its presence in one of the limiting cases of the closed form solutions to be presented below. The isolated blade lag mode is also identical with the reactionless differential collective rotor lag mode, "L1D" of the 2GCHAS model.

Since the symmetry of the blades' motions prevents hub motion, these roots are well approximated by constraining the hub motion $\Psi_H = \Omega t$ with Ω constant. This important mode's behavior can be approximated by $I_H \to \infty$ or by $K_S \to \infty$ in Eq. (25) or with the transformation $\psi = T\psi'$ where $T = [0, 0, 0, 0, 1]^T$, any of which leads to the equation for the roots

$$\lambda^2 M_B \frac{l^2}{3} + \lambda C_B + K_{B\Omega} = 0 \tag{31}$$

The roots can be determined from the quadratic formula as

$$\lambda = \frac{-C_B}{2M_B \frac{l^2}{3}} \pm \frac{\sqrt{C_B^2 - 4M_B \frac{l^2}{3}(M_B \Omega^2 \frac{l}{2} e + K_B)}}{2M_B \frac{l^2}{3}} \tag{32}$$

Setting the discriminant to zero leads to the critical value for Ω

$$\Omega_{crit} = \sqrt{\frac{2}{M_B l e}} \sqrt{\frac{C_B^2}{4M_B \frac{l^2}{3}} - K_B} \tag{33}$$

For $\overline{\Omega} > \overline{\Omega}_{crit}$, the real part of the root is

$$\sigma = \frac{-C_B}{2M_B \frac{l^2}{3}} \tag{34}$$

Similarly, for $\overline{\Omega} \to 0$ and $K_B \to 0$, the two roots are real. One is $\lambda = 0$, as is computed. And the other is

$$\lambda_4 = \frac{-C_B}{M_B \frac{l^2}{3}} \tag{35}$$

Finally, the asymptote as $\Omega \to \infty$ of the frequency of the conjugate pair is

$$\omega = \pm i\Omega\sqrt{\frac{3e}{2l}} \tag{36}$$

This is the traditional isolated blade lag frequency for an offset hinged articulated rotor.

Evaluating Eq. (33) gives $\overline{\Omega}_{crit} = 0.25$, which is very close to the point at which the computed "L1D" roots change from two real roots to a complex conjugate pair (see Fig. 4). Evaluating Eq. (34) gives $\overline{\sigma} = -0.677$, which is very close to the computed value (see the damping for "L1D" in Fig. 4). Evaluating Eq. (35) gives $\overline{\lambda} = -1.35$ which is very close to the computed value and can be identified as the y-axis intercept of the lower of the "L1D" roots in Fig. 4. Evaluating Eq. (36) gives $\overline{\omega} = 0.271\overline{\Omega}$. This asymptote is also consistent with Fig. 4.

Rotor/Engine/Transmission Modes

The "Rotor/Engine/Transmission pair" is weakly coupled with the smaller of the "Hub real roots" for $0 \leq \overline{\Omega} <\sim 1$. Nonetheless, it is useful to approximate the behavior for high rotor speed by assuming the only flexibility is in the rotor shaft (i.e., the engine is rigidly geared to the transmission and the blade is rigidly connected to the hub by virtue of centrifugal stiffening at high rotor speed). In this case, the space of possible displacements is spanned by the two possible "rigid body" motions previously defined in Eq. (6) plus a rigid body rotation of the rotor only. In this case, the transformation $\psi = T\psi'$ constraining the motion to the desired subspace is

$$T = \frac{1}{\sqrt{I_{Rc}}} \begin{bmatrix} 1 & 1 - \frac{I_{Rc}}{I_F - (N-1)I_B} & 0 \\ \frac{1}{N} & \frac{1}{N} + \frac{(N-1)I_{Rc}}{N[I_F - (N-1)I_B]} & 0 \\ 1 & 1 & 0 \\ 1 & 1 & \frac{\sqrt{I_{Rc}}}{\sqrt{I_{Rtr}}} \\ 1 & 1 & \frac{\sqrt{I_{Rc}}}{\sqrt{I_{Rtr}}} \end{bmatrix} \tag{37}$$

Transforming the mass, damping and stiffness matrices (Eqs. (3), (4) and (5)) by postmultiplying by T and premultiplying by its transpose and then taking the determinant in the generalized eigenvalue problem gives the following equation for the roots

$$\begin{aligned} &\lambda^6\{(I_{Rc} - I_{Rtr})[I_F + (N-1)^2 I_E] - [I_F - (N-1)I_E]^2\} \\ &+\lambda^5 (I_{Rc} - I_{Rtr}) N^2 C_E \\ &+\lambda^4 \tfrac{K_S}{I_{Rtr}}\{I_{Rc}[I_F + (N-1)^2 I_E] - [I_F - (N-1)I_E]^2\} \\ &+\lambda^3 \tfrac{K_S}{I_{Rtr}} I_{Rc} N^2 C_E = 0 \end{aligned} \tag{38}$$

Clearly there is a root at $\lambda = 0$ with a multiplicity of three. The other three roots are found using the cubic formula with the approximations $I_T \ll I_F$; $I_E \ll I_F$; $I_E N^2 \ll I_F$; and $C_E^2 \ll K_E I_E$ as was done previously (Eqs. (12)–(22)). An algebraic expression for the fourth root is not presented since a slightly better approximation was obtained previously as Eq. (8). With the above approximations, the following algebraic expression are obtained for the fifth and sixth "Rotor/Engine/Transmission" roots

$$\begin{aligned} \lambda_5, \lambda_6 \approx & -\frac{C_E N^2 I_{Rtr}}{2(I_{Rtr} + I_E N^2 + I_T)(I_E N^2 + I_T)} \\ & \pm i\sqrt{\frac{K_S[I_{Rtr} + (I_E N^2 + I_T)]}{I_{Rtr}(I_E N^2 + I_T)}} \end{aligned} \tag{39}$$

Evaluating Eq. (39) gives $\overline{\lambda}_5, \overline{\lambda}_6 = -.0228 \pm .558i$ which is very close to the computed values $\overline{\lambda}_5, \overline{\lambda}_6 = -.0232 \pm .550i$ at $\overline{\Omega} = 5$. This is a very close approximation to the "Rotor/Engine/Transmission pair" (Fig. 6) for larger $\overline{\Omega}$.

Undamped Rotor/Engine/Transmission Modes

It is of interest to develop closed form expressions for the coupled "Rotor/Engine/Transmission" and "Hub" root frequencies and asymptotes at low and high rotor speeds. Such expressions are easily derived for the undamped configuration, $C_E = C_B = 0$. The "Rotor/Engine/Transmission pair" and the "Hub real roots" are coupled for smaller $\overline{\Omega}$. But other than the brief strong coupling with the "Engine real root" are uncoupled from the rest of the roots. Most of the behavior is well approximated by assuming there is zero fuselage motion and that the engine is constrained to move with the transmission (through the gear ratio N). In this case, the transformation $\psi = T\psi'$ constrains the motion to the desired subspace if

$$T = \begin{bmatrix} 0 & 0 & 0 \\ 1 & 0 & 0 \\ 1 & 0 & 0 \\ 0 & 1 & -N_B M_B(\frac{l^2}{3} + \frac{l}{2}e) \\ 0 & 1 & N_B M_B(\frac{l}{2}e + e^2) + I_H \end{bmatrix} \tag{40}$$

The presence of three active degrees of freedom, the blade, the hub and the transmission/engine combination would lead to a sixth order polynomial with only one zero root—difficult to solve analytically. So, it will be further assumed that the damping terms C_E and C_B are zero. Assuming the damping matrix is zero and transforming the mass and stiffness matrices (Eqs. (3) and (5)) by postmultiplying by T and premultiplying by its transpose and then taking the determinant in the generalized eigenvalue problem gives the following equation for the roots

$$\lambda^6 a + \lambda^4 b + \lambda^2 c = 0 \tag{41}$$

where

$$a = I_{Rtr} N_B M_B \frac{l^2}{3}(N^2 I_E + I_T)(I_H + N_B M_B \frac{e^2}{4}) \tag{42}$$

$$\begin{aligned} b = & I_{Rtr}^2 (N^2 I_E + I_T) N_B K_{B\Omega} \\ & + [N_B M_B(\frac{l^2}{3} + \frac{l}{2}e)]^2 (N^2 I_E + I_T) K_S \\ & + (I_{Rtr} + N^2 I_E + I_T) N_B M_B \frac{l^2}{3}(I_H + N_B M_B \frac{e^2}{4}) K_S \end{aligned} \tag{43}$$

$$c = (I_{Rtr} + N^2 I_E + I_T) I_{Rtr} N_B K_{B\Omega} K_S \tag{44}$$

Clearly there is a root at $\overline{\lambda} = 0$ with multiplicity two. The other four roots can be obtained by applying the quadratic formula to $a\lambda^4 + b\lambda^2 + c$ to obtain values for λ^2 and then taking the square root. It is easily seen that in the limit as $\Omega \to \infty, b^2 \gg 4ac$. It is also easily seen that in the limit as $K_{B\Omega} \to 0, b^2 \gg 4ac$. If some additional approximations are made which are appropriate for typical rotorcraft (e.g., $e \ll l$, $I_H \ll N^2 I_E + I_T$), it is generally true that $b^2 \gg 4ac$. Using the approximation $\sqrt{1-\epsilon} \approx 1 - \epsilon/2$ the formula for the roots are $i\sqrt{c/b}$ and $i\sqrt{b/a}$. So the frequencies in terms of Eqs. (42), (43) and (44) are $\pm i\sqrt{c/b}$ and $\pm i\sqrt{b/a}$. This gives for the third and fourth "Rotor/Engine/Transmission" roots

$$\lambda_3, \lambda_4 \approx \pm i\sqrt{\frac{\frac{(I_{Rtr} + N^2 I_E + I_T) I_{Rtr}}{(N^2 I_E + I_T)} N_B K_{B\Omega} K_S}{I_{Rtr}^2 N_B K_{B\Omega} + [N_B M_B(\frac{l^2}{3} + \frac{l}{2}e)]^2 K_S}} \tag{45}$$

and for the fifth and sixth "Hub" roots

$$\lambda_5, \lambda_6 \approx \pm i\sqrt{\frac{N_B M_B \frac{l^2}{3}(N^2 I_E + I_H + N_B M_B \frac{e^2}{4}) K_S + I_{Rtr}(N^2 I_E + I_T) N_B K_{B\Omega}}{N_B M_B \frac{l^2}{3}(N^2 I_E + I_T)(I_H + N_B M_B \frac{e^2}{4})}} \tag{46}$$

In the limit as $\Omega \to \infty$ the formulas for the "Rotor/Engine/Transmission" roots become

$$\lambda_3, \lambda_4 \approx \pm i\sqrt{\frac{K_S[I_{Rtr} + (I_E N^2 + I_T)]}{I_{Rtr}(I_E N^2 + I_T)}} \tag{47}$$

which is the undamped analog of Eq. (39). This frequency can be thought of as the free-free mode of the rotor inertia reacting against the engine and transmission inertia through the rotor shaft spring, since the centrifugal stiffening effectively locks out lag hinge motion as rotor speed becomes large. It represents the high rotor speed limit of the basic mode of rotor/engine/drive train dynamics. The formulas for the "Hub" become

$$\lambda_5, \lambda_6 \approx \pm i\Omega\sqrt{\frac{3e}{2l}}\sqrt{\frac{I_{Rtr}}{I_H + N_B M_B \frac{e^2}{4}}} \tag{48}$$

which is the undamped analog of Eq. (30).

For $K_B = 0$ and in the limit as $\Omega \to 0$ the formula for the "Rotor/Engine/Transmission" roots, Eq. (45) becomes

$$\lambda_3, \lambda_4 \approx \pm i\Omega\sqrt{\frac{3e}{2l}}\sqrt{\frac{I_{Rtr} + I_E N^2 + I_T}{I_E N^2 + I_T}} \tag{49}$$

Note that this expression provides the low rotor speed asymptote for the basic coupled mode of rotor/engine/drive train dynamics and it reveals the central role of the isolated blade lag frequency in the coupled rotor/drive train dynamics. The isolated blade lag frequency $\omega = \Omega\sqrt{\frac{3e}{2l}}$ (Eq. (36)), is amplified as the isolated rotor boundary condition is relaxed to the inertial restraint of the drive train.

In the limit as $K_{B\Omega} \to 0$ Eq. (46) provides the y-axis intercept for "Hub" roots as

$$\lambda_5, \lambda_6 \approx \pm i\sqrt{\frac{[(N^2 I_E + I_T) + (I_H + N_B M_B \frac{e^2}{4})] K_S}{(N^2 I_E + I_T)(I_H + N_B M_B \frac{e^2}{4})}} \tag{50}$$

and the slope at that point is zero.

Parametric Investigations

To provide further insight into the fundamental dynamic behavior of rotorcraft, and to investigate a wider range of rotorcraft, a large number of parametric variations were performed. Results and their interpretation for some of the more important configurations are reported below.

Blade Lag Damping Variation

The behavior of the REDT model was investigated for a variety of blade lag-damping, C_B, values. It was found that, compared to the behavior of the "Rotor/Engine/Transmission pair" and the "Hub pair" for nominal values, the character of the coupling between an articulated rotor and an engine/drive train is significantly influenced by smaller values of C_B. Results

for small blade lag-damping permits the behavior of the modes to be more clearly observed and easily understood, particularly with regard to several of the approximate closed form solution results. (cf. "Undamped Rotor/Drive Train Modes"). The eigenvalue behavior for the blade lag damper decreased to 10% of the nominal value is presented in Fig. 9. Comparing this behavior with the nominal results, Fig. 6, noting the difference in scales, the following can be observed.

The "Hub pair" is oscillatory at all rotor speeds with C_B at 10% whereas with C_B at 100% damping it was overdamped for $\overline{\Omega} < 3$. Note that the damping of the "Hub pair" is reduced by a factor of 10 with C_B at 10%. The high rotor speed behavior of the "Hub pair" for C_B at 10% is consistent with the asymptotes given by Eqs. (30) or (48) and the low rotor speed behavior is consistent with the asymptote given by Eq. (50).

With C_B at 10% the "Rotor/Engine/Transmission pair" is overdamped for $\overline{\Omega} < 0.02$, and becomes oscillatory for $\overline{\Omega} > 0.02$ but was oscillatory at all rotor speeds for C_B at 100%. At low rotor speed, the "Rotor/Engine/Transmission pair" is more heavily damped with C_B at 100% and even for rotor speed 1.0, the damping is over twice the damping with C_B at 10%, indicating the beneficial effect of blade lag dampers on drive train stability. At low rotor speeds the character of the mode is that of an uncoupled rotor collective lag mode amplified due to the relaxation of the boundary condition to an inertial restraint (see the asymptote given by Eq. (49) and the accompanying discussion). As rotor speed begins to increase it becomes asymptotic to a frequency of about 0.5 as determined by the drive train inertia and stiffness consistent with Eq. (39) or (47).

The "Engine/Transmission" pair and the "Engine real root" are generally not sensitive to the blade damper value as indicated by the closed form solutions. However, at low rotor speed, the "Engine real root" convergence mode for C_B at 10% couples with one of the overdamped "Rotor/Engine/Transmission pair", rather than one of the "Hub real roots" as in the C_B at 100% configuration.

Hingeless Rotor Variation

One important class of rotorcraft whose dynamics are not well represented by the nominal parameters is rotorcraft with hingeless rotors. A soft in-plane hingeless rotor can be simulated with a lag-hinge spring in combination with a smaller lag damper (since the lag damper on a hingeless rotor is typically much smaller than that on an articulated rotor). A lag-hinge spring was selected which provided an undamped nonrotating isolated blade lag frequency of 0.5/rev. Inverting Eq. (32) and assuming C_B is very small, $K_B = (0.5\Omega_0)^2 M_B \frac{l^2}{3} = 295858$. At $\overline{\Omega} = 1$ the fixed hub frequency rises to 0.57/rev. The lag-damper value (C_B) was set to 5% of the nominal value. The results of using these parameter values in the REDT model are presented in Fig. 10.

The most distinctive feature is the absence of coupling between the "Rotor/Engine/Transmission pair" and any other modes, resulting from the very small C_B and the presence of K_B making the behavior more like that at high $\overline{\Omega}$ for the nominal case.

The differences in the behavior of the "Hub pair" can best be understood by comparison with the previous C_B at 10% results (Fig. 9). As would be expected from Eq. (28), the 50% smaller blade lag damper results in a 50% smaller damping for the mode. And, as would be expected from Eq. (46), the presence of K_B here increases $K_{B\Omega}$ making the frequencies for the hingeless case like the those for the C_B at 10% case at higher $\overline{\Omega}$.

The only other behavior of interest is the slight coupling of the "Engine/Transmission pair" and the "Hub pair" where their frequencies cross near $\overline{\Omega} = 3.2$. The coupling results in some sharing of the damping so that there is a slight decrease in the larger damping of the "Hub pair" and a slight increase in the smaller damping of the "Engine/Transmission pair" as the roots cross.

Engine Variation

Although the nominal engine parameters were chosen to be representative of realistic rotorcraft engines, configurations may vary widely. To investigate how the engine/drive train dynamic behavior can be affected, a wide variety of configurations were investigated. One configuration, which led to simultaneous coupling of the "Engine real root," the "Hub real root" and the "Rotor/Engine/Transmission pair", was for $I_E = 2(\approx 16\times$ nominal) and $C_E = 7(\approx 20\times$ nominal). A comparison of the results obtained with the simplified REDT model and the comprehensive 2GCHAS model for this configuration is presented in Fig. 11. It can be seen that the frequencies for the roots labeled "Hub/Engine pair" and the roots labeled "Rotor/Engine/Transmission pair" in the REDT model cross, whereas the dampings remain separated. (Note that the branches of the roots are labeled according to their dominant character well away from the region of heavy coupling where the changing character of the modes makes them difficult to identify.) Conversely, in the 2GCHAS model, the frequencies of the roots labeled "Eng/Hub pair" and "Rtr/Eng/Trn pair" remain separated and it is the dampings that cross.

A magnified view of the crossing is presented for the REDT model along with similar plots for slightly smaller damping, $C_E = 6$ in Fig. 12. The magnified presenta-

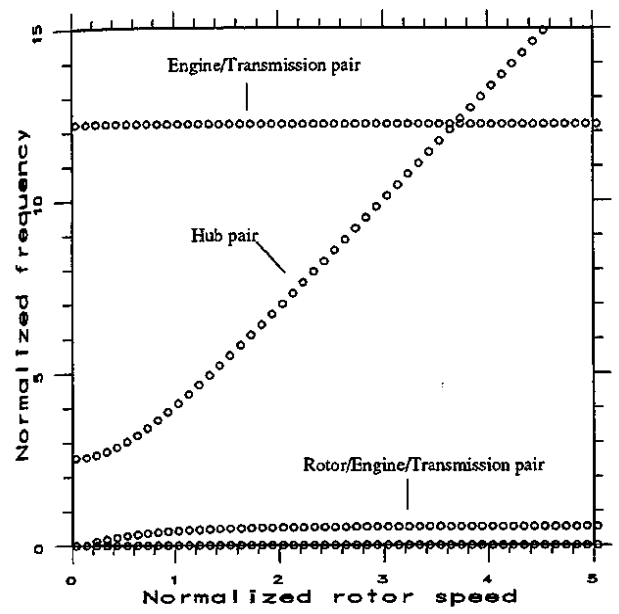

(a) Frequency of all roots

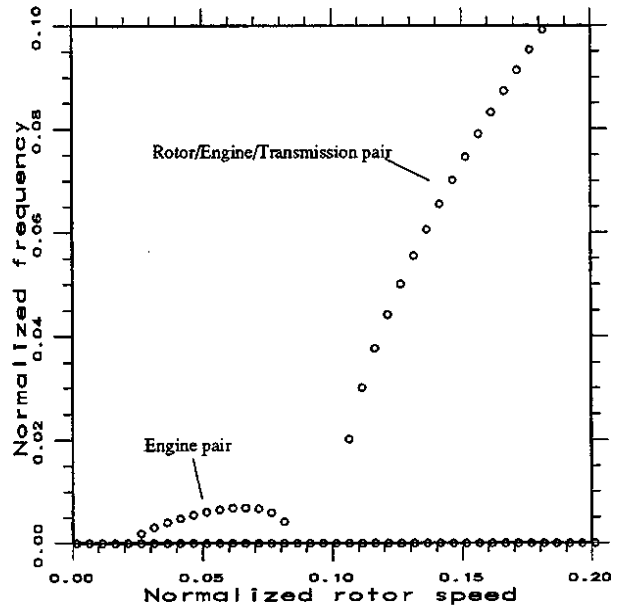

(b) Frequency of smaller roots

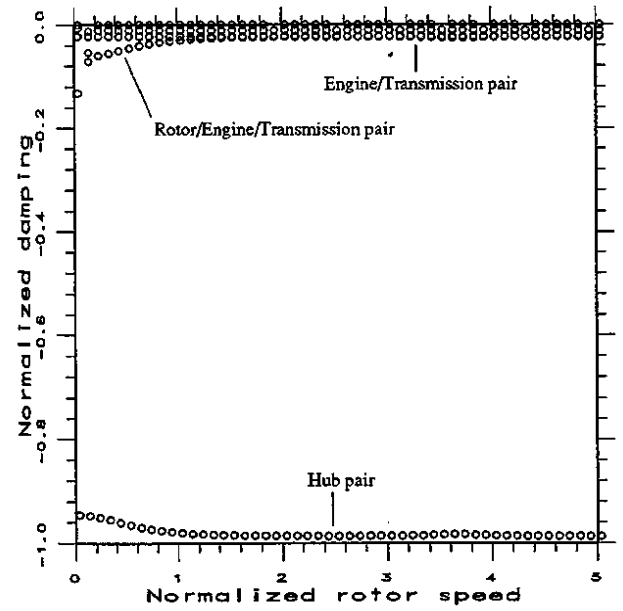

(c) Damping of all roots

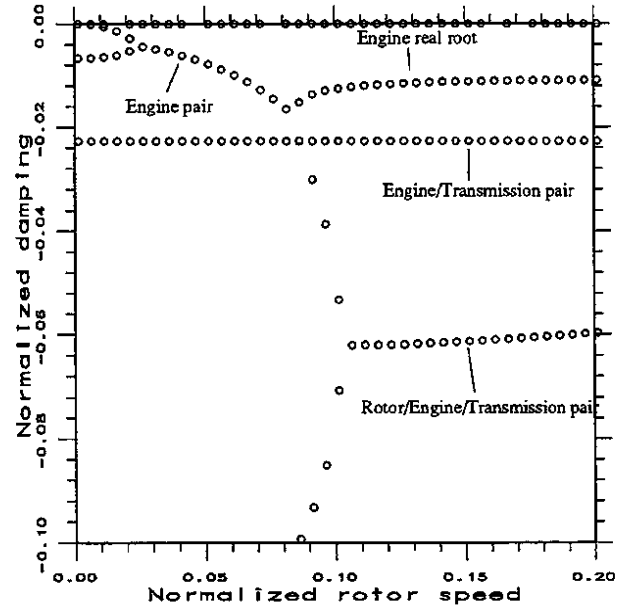

(d) Damping of smaller roots

Figure 9: Eigenvalues for REDT model with $C_B = 10\%$ of nominal

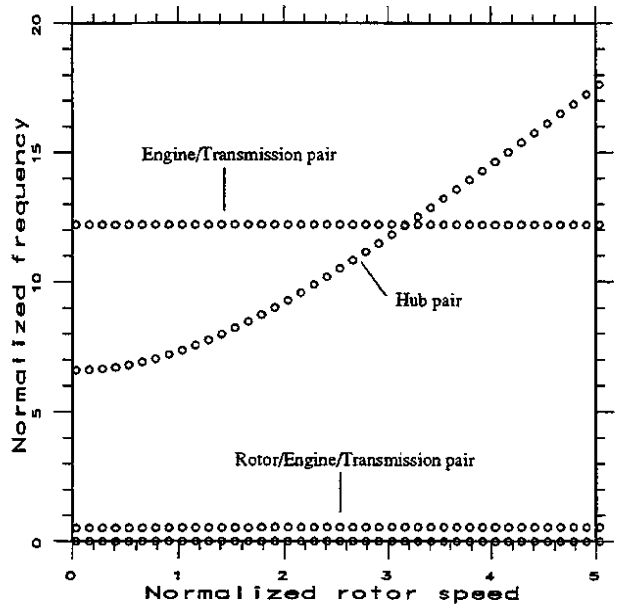

(a) Frequency

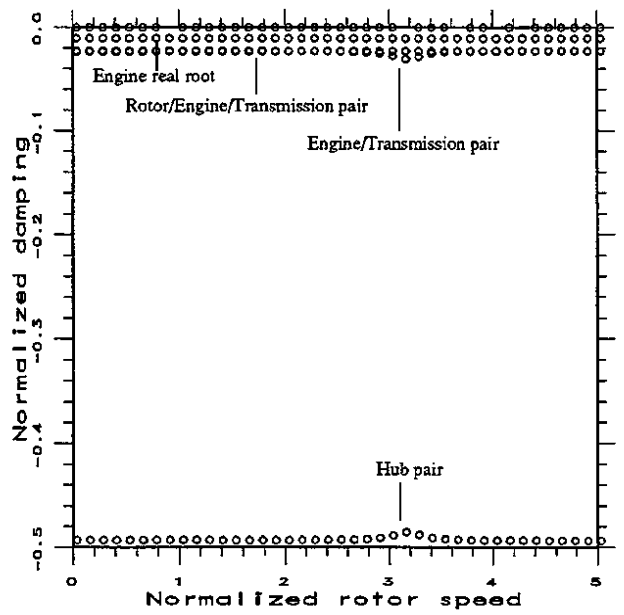

(b) Damping

Figure 10: Eigenvalues for a simulated hingeless rotor REDT model (C_B at 5% and 0.5/rev nonrotating lag frequency)

tion makes it clear that the for the REDT model, the frequencies are crossing for $C_E = 7$ and are remaining separate for $C_E = 6$ and that conversly, the dampings remain separate for $C_E = 7$ and cross for $C_E = 6$. Thus the behavior of the 2GCHAS model with $C_E = 7$ is very close to that of the REDT model with $C_E = 6$.

Tail Rotor Variation

To gauge the effects of tail rotor dynamics on the system frequencies, the comprehensive model for the nominal case was analyzed with the tail rotor spring made effectively rigid ($K_{TR} = 2 \times 10^8 = 10^5 \times$ nominal). The corresponding frequency and damping plots are shown in Fig. 13. Comparing these results to the nominal case (see Fig. 4) shows that the frequency of the "Rtr/Eng/Trn pair" decreases noticeably, while the damping of that mode increases, except near $\overline{\Omega} = 1.0$. Stiffening K_{TR} brings the 2GCHAS and REDT models into closer correspondence, and a careful comparison of Figs. 4, 13, and 6b shows that that change improves the agreement between the 2GCHAS and REDT results, especially for the "Rtr/Eng/Trn pair." Tail rotor dynamics are often omitted from engine models (see, for example, Ref. [14]), and the results here suggest that while that is a reasonable first approximation, it may not be adequate for refined analyses.

Engine Feedback Gain Variation

The effects of varying feedback gain may be observed by examining Figs. 4, 14 and 15, which present eigenalysis results for $G = 10$ (nominal), 200, and 1000. The figures show that the damping of the "Eng real root" increases with feedback, but the damping of the "Tail rtr" mode and the "Rtr/Eng/Trn pair" decrease with increasing feedback. In fact, it is apparent from Fig. 15 that for $G = 1000$, the "Rtr/Eng/Trn pair" is unstable when $\overline{\Omega} < .5$.

The results also show that an increase in G affects interference of the "Eng real root" and "Hub real root" in a manner that is analogous to an increase in engine damping, C_E. This is apparent from comparing Figs. 14 and 15 with Fig. 11. All these figures are characterized by the coalesence of the "Eng real root" and the higher "Hub real root" into an "Eng/Hub pair" at intermediate values of $\overline{\Omega}$, and the re-emergence of pure real roots at high values of $\overline{\Omega}$.

Concluding Remarks

This study has sought to develop an understanding of coupled rotor/engine/drive train/fuselage dynamics. To

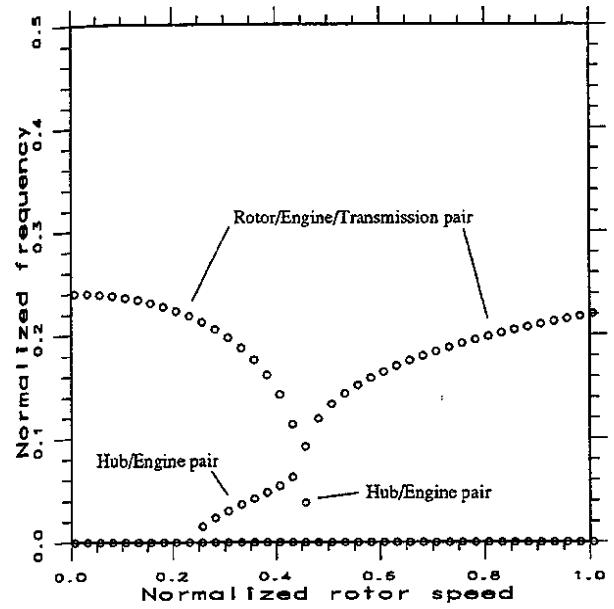

(a) REDT frequency of small roots

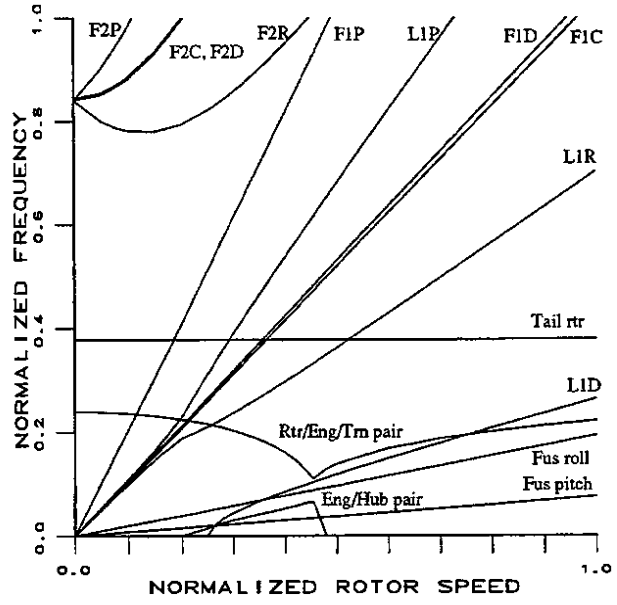

(b) 2GCHAS frequency of roots

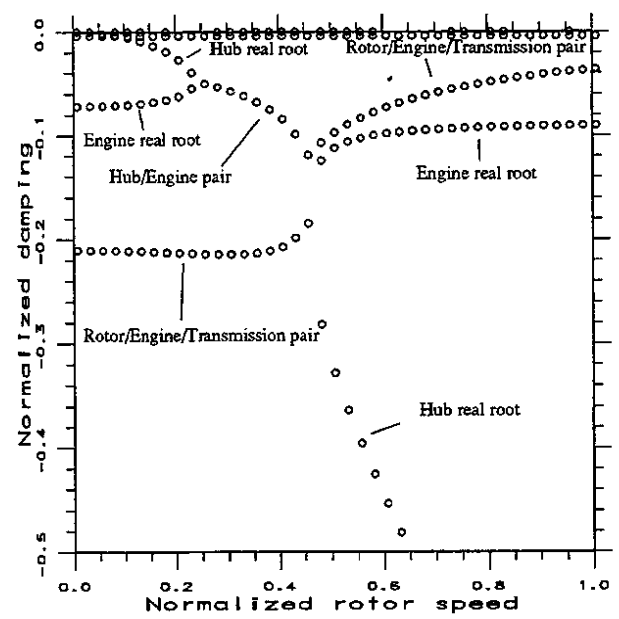

(c) REDT damping of small roots

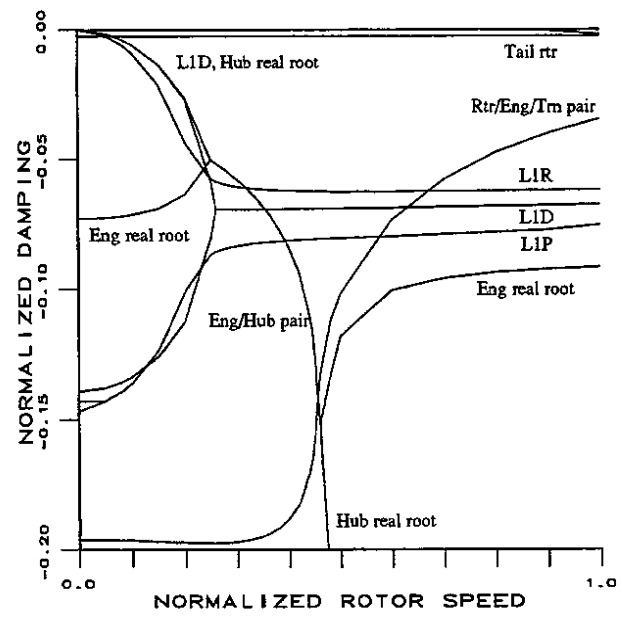

(d) 2GCHAS damping of roots

Figure 11: Comparison of smaller eigenvalues from REDT and 2GCHAS for strongly coupled engine with $I_E = 2$ and $C_E = 7$.

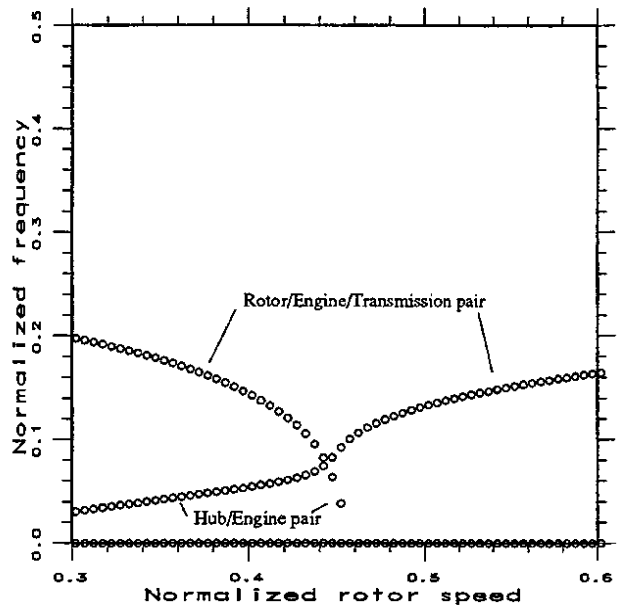

(a) Frequency of small roots for $C_E = 7$

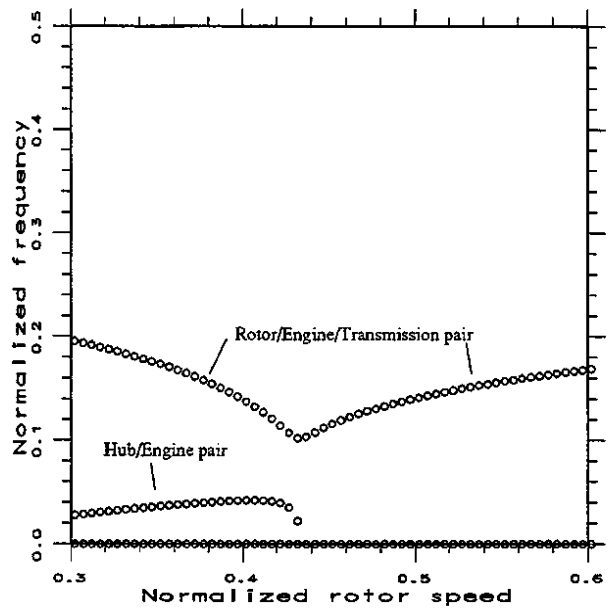

(b) Frequency of small roots for $C_E = 6$

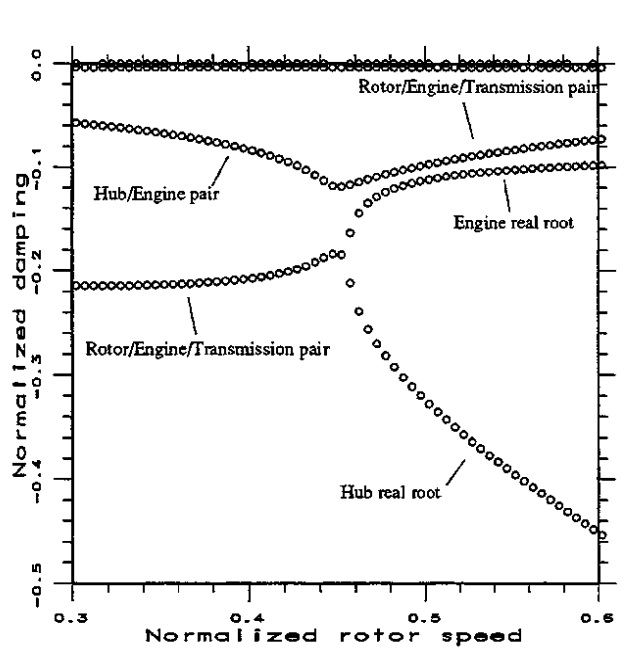

(c) Damping of small roots for $C_E = 7$

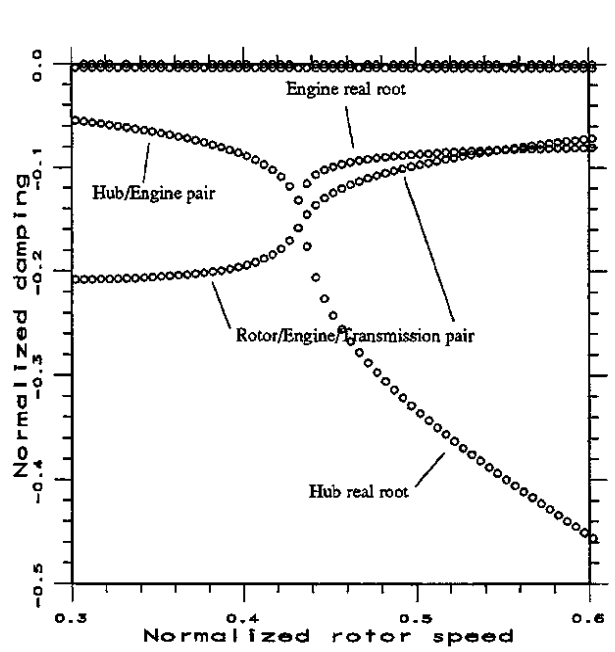

(d) Damping of small roots for $C_E = 6$

Figure 12: Eigenvalues for REDT model with a strongly coupled engine $I_E = 2$ and $C_E = 7$ or $C_E = 6$—magnified

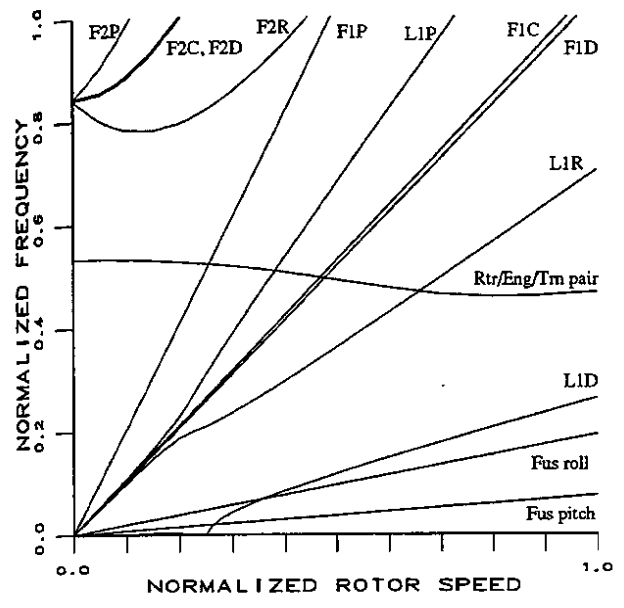

(a) Frequency

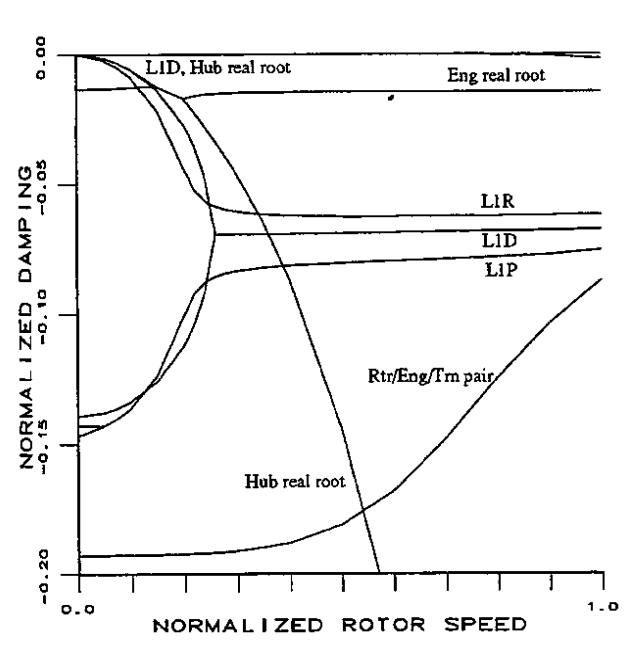

(b) Damping

Figure 13: Eigenvalues for 2GCHAS model with rigid tail rotor shaft spring.

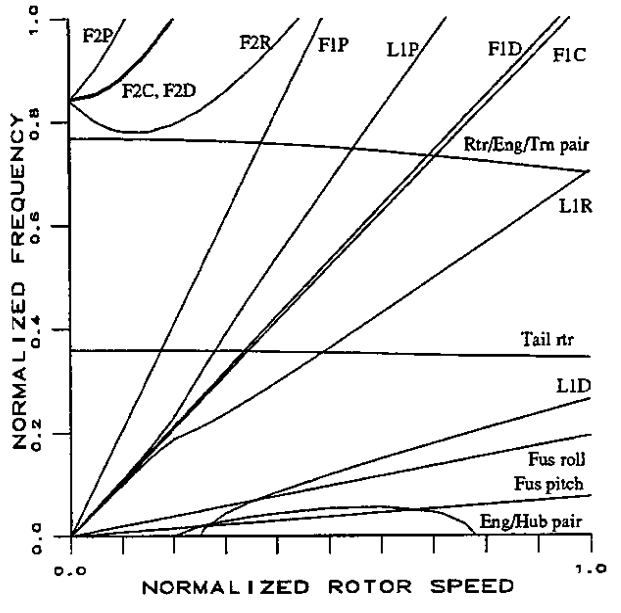

(a) Frequency

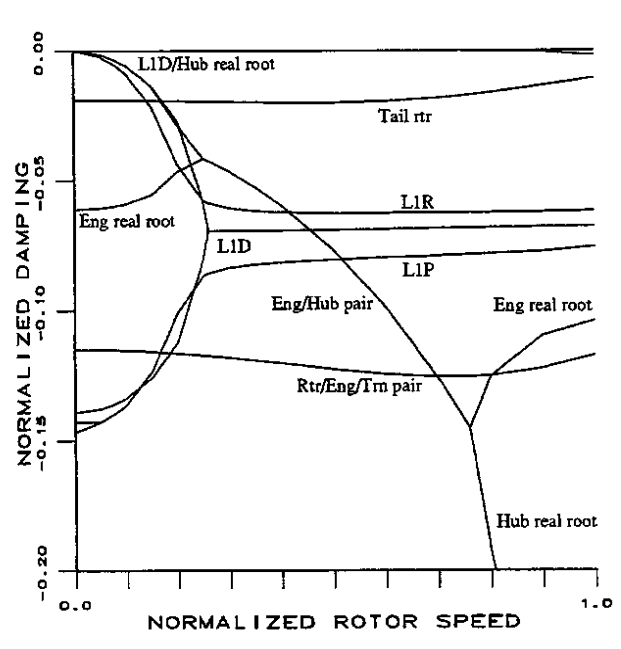

(b) Damping

Figure 14: Eigenvalues for 2GCHAS model with engine feedback gain $G = 200$.

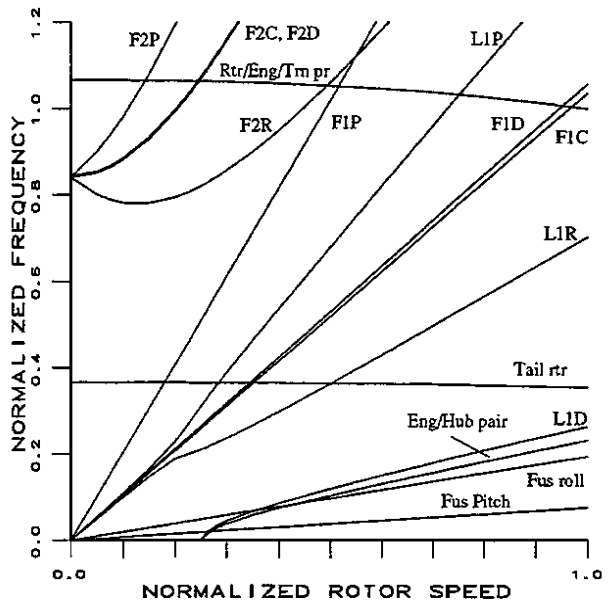

(a) Frequency

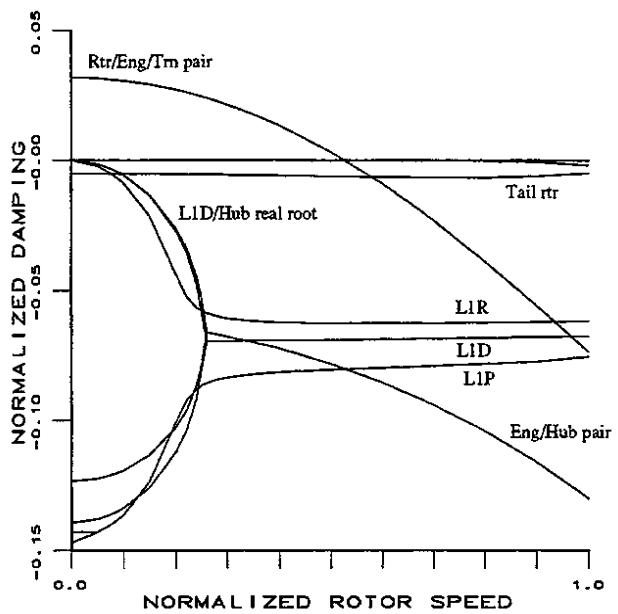

(b) Damping

Figure 15: Eigenvalues for 2GCHAS model with engine feedback gain $G = 1000$.

that end, a model of a system incorporating these components was developed using the 2GCHAS comprehensive rotorcraft code. The eigenanalyses of this model revealed complex interactions among the components, and the makeup of these modes sometimes exhibit significant changes as rotor speed varies. The simplified REDT analytical model was introduced to complement 2GCHAS in the course of this study and permit a more detailed exploration of the system's basic modal characteristics.

The results of the comprehensive analyses were verified with an analysis of a simplified five degree of freedom model. The study of the simplified model showed that the rotor/engine/drive train modes are often dominated by one portion of the system acting in isolation from the other parts. Approximate closed form solutions gave excellent agreement for the isolated frequencies, and further verified the results of the comprehensive and simplified models.

Parameter studies were conducted for the comprehensive and simplified models involving blade damping, hingeless rotor lag stiffness, engine parameters, and engine controller feedback. The analytical model accurately predicted the effects of system parameters on modes with little or no coupling, but the regions of significant modal interaction were found for some values of engine mass and damping properties.

This study demonstrates how comprehensive models and computer programs such as 2GCHAS, simplified models and computer programs such as REDT, closed form analyses and parametric studies complement one another in gaining insight into the fundamental dynamic behavior of rotorcraft.

References

[1] Twomey, W. J. and Ham, E. H.; "Review of Engine/Airframe/Drive Train Dynamic Interface Development Problems," USARTL-TR-78-13, June 1978.

[2] Richardson, D.A. and Alwang, J.R.; "Engine/Airframe/Drive Train Dynamic Interface Documentation," USARTL-TR-78-11, April 1978.

[3] Hanson, H.W.; Balke, R.W.; Edwards, B.D.; Riley, W.W.; and Downs, B.D.; "Engine/Airframe/Drive Train Dynamic Interface Documentation," USARTL-TR-78-15, October 1978.

[4] Kuczynski, W.A.; Cooper, D. E.; Twomey, W.J.; and Howlett, J.J.; "The Influence of Engine/Fuel Control Design on Helicopter Dynamics and Handling Qualities," Journal of the American Helicopter Society, Vol. 25, No. 2, April 1980.

[5] Shanthakumaran, P.; Harding, T.; Thompson, T.; Kuehn. M.; and Monroe, D.; "Flight Simualation Model Application for AH-64A Apache Engine Integration," Proceedings 49th Annual Forum Of the American Helicopter Society, St. Louis, MI, May 19-21, 1993.

[6] Ballin, Mark G., "A High Fidelity Real-Time Simulation of a Small Turboshaft Engine," NASA TM 100991, July 1988.

[7] Warmbrodt, W.; and Hull, R.; "Development of a Helicopter Rotor/Propulsion System Dynamics Analysis," Paper AIAA-82-1078 presented at the AIAA/SAE/ASME 18th Joint Propulsion Conf., Cleveland, Ohio, June 21-23, 1982.

[8] Ockier, Carl J. and Celi, Roberto, "Dynamics and Aeroelasticity of a Coupled Helicopter Rotor-Propulsion System in Hover," Paper AIAA-91-1220-CP

[9] Jaw, Link C. and Bryson, Arthur E., "Modeling Rotor Dynamics with Rotor Speed Degree of Freedom for Drive Train Torsional Stability Analysis," Paper presented at the 16th European Rotorcraft and Powered Lift Forum, Glasgow Scotland, Sept. 19–21, 1990

[10] Ormiston, R.A.; *et. al.* "Comprehensive Aeromechanics Analysis of Complex Rotorcraft Using 2GCHAS," Paper PS1 presented at the American Helicopter Society Aeromechanics Specialists Conference, San Francisco, CA, 1994.

[11] Anon., "2GCHAS Theory Manual," USAATCOM Technical Memorandum 93-A-004, U.S. Army Aviation and Troop Command, CA, 1993.

[12] Anon., "2GCHAS User's Manual," USAATCOM Technical Memorandum 93-A-002, U.S. Army Aviation and Troop Command, CA, 1993.

[13] Anon., "2GCHAS Applications Manual," USAATCOM Technical Memorandum 93-A-001, U.S. Army Aviation and Troop Command, CA, 1993.

[14] Neff, J.R., and Walton, R.P., "Engine/Rotor Torsional Compatibility Data, YAH-64 Advanced Attack Helicopter, Report No. 77-V-1401-2, Hughes Helicopters, Inc., April, 1978.